AFRL-SR-AR-TR-05-

0043

REPORT DOCUMENTATION PAGE

1. REPORT DATE *(DD-MM-YYYY)*	2. REPORT TYPE	3. DATES COVERED *(From - To)*
	Final Report	15 Oct 2003 - 14 Jul 2004

4. TITLE AND SUBTITLE
Induction-Based Thermographic Inspection of Composites

5a. CONTRACT NUMBER

5b. GRANT NUMBER
FA9550-04-C-0009

5c. PROGRAM ELEMENT NUMBER

6. AUTHOR(S)
Steven M. Shepard

5d. PROJECT NUMBER

5e. TASK NUMBER

5f. WORK UNIT NUMBER

7. PERFORMING ORGANIZATION NAME(S) AND ADDRESS(ES)
Thermal Wave Imaging Inc.
845 Livernois Street
Ferndale MI 48220-2308

8. PERFORMING ORGANIZATION REPORT NUMBER

9. SPONSORING/MONITORING AGENCY NAME(S) AND ADDRESS(ES)
USAF/AFRL
AFOSR
801 N. Randolph Street
Arlington VA 22203

NA

10. SPONSOR/MONITOR'S ACRONYM(S)
AFOSR

11. SPONSOR/MONITOR'S REPORT NUMBER(S)

12. DISTRIBUTION/AVAILABILITY STATEMENT

Distribution Statement A. Approved for public release; distribution is unlimited.

13. SUPPLEMENTARY NOTES

14. ABSTRACT

The ultimate assessment of feasibility was determined in the final task; however, the tasks preceding it were required in order to construct an optimized test system. Our expectation at the outset of the projects was that the combination of induction heating and thermography would outperform systems based exclusively on either electromagnetic induction or thermography. The rationale was that the combined system would offer better capabilities for wide area inspection of large structures than induction systems, and better sensitivity to deep, low aspect ratio indications than pulsed thermography. Ultimately, the results of the experiments in Task 4 did not entirely support our initial optimism. Although the proof-of-principal system did offer the anticipated advantages for side area inspection, the sensitivity of the system did not exceed that of current pulsed thermography capabilities, and in fact, did not perform as well in some key respects. Although some aspects of the performance of the SIT system could perhaps be attributed to shortcomings in the design or construction of this first demonstration unit, analysis of the data indicates that some important limitations of the approach are fundamental.

15. SUBJECT TERMS

16. SECURITY CLASSIFICATION OF:			17. LIMITATION OF ABSTRACT	18. NUMBER OF PAGES	19a. NAME OF RESPONSIBLE PERSON
a. REPORT	b. ABSTRACT	c. THIS PAGE			19b. TELEPHONE NUMBER *(Include area code)*
UU	UU	UU	UU	30	

Development of NDE Technique with Induction Heating and Thermography on Conductive Composite Materials

Steven M. Shepard, James R. Lhota and Tasdiq Ahmed

Thermal Wave Imaging, Inc., Ferndale, Michigan

HeeJune Kim, Shridhar Yarlagadda and John W. Gillespie, Jr.

University of Delaware Center for Composite Materials (UD-CCM), Newark, Delaware

Introduction

In this Phase I STTR program, Thermal Wave Imaging, Inc. (TWI) and the University of Delaware Center for Composite Materials (UD-CCM) have collaborated to investigate the feasibility of Thermographic Nondestructive Evaluation (TNDE) of carbon fiber composite structures using induction heating as the excitation method. The technique relies on the hypothesis that low-power induction heating of the sample generates additional small levels of local 3-D volumetric heating near defects at or beneath the surface, and the resulting anomalies in the surface temperature profile are detectable by dedicated signal processing algorithms based on the anticipated diffusion process. The 3-D heat generation profile is a function of the inherent carbon fiber-based electrical resistance network in the composite, and any changes in the network due to damage or defects affect heat generation capability (pattern and temperature). In addition, the presence of damage or defects will cause localized magnetic flux concentrations resulting in localized heating at the defect. In the proposed technique, the relative positions of the infrared (IR) camera and the and induction coil are fixed, and the entire assembly moves relative to the sample. Processing routines are used to deconvolve the relative motion, and the stationary reconstructed sequence is further processed to identify areas where anomalies in surface temperature cooling rates occur.

The proposed technique offers the possibility of several significant improvements to current inspection techniques, including the elimination of interconnects and embedded sensors, scanning of large surface areas rapidly, usability with current in-service structures and the use of industry standard induction and IR detection hardware. In particular, the technique may significantly improve the performance of pulsed thermography. Although the use of pulsed thermography for NDT of carbon fiber composites has increased significantly in the past 10 years, features with aspect ratios (diameter / depth) <~ 1-2 are typically considered undetectable, despite numerous advances in thermographic signal processing. The use of induction heating instead of optical flash heating allows a more direct interaction with subsurface defects, which may improve sensitivity and the limits of detectability of low-aspect ratio defects.

Executive Summary of Phase I Results

Activity in the Phase I program was concentrated on 4 key task areas:

1. Modeling of induction heating in carbon fiber composites
2. Development of a proof-of-principle Scanning Induction Thermography (SIT) system
3. Signal processing of SIT data
4. Experimental evaluation of carbon fiber samples using the SIT system

The ultimate assessment of feasibility was determined in the final task; however, the tasks preceding it were required in order to construct an optimized test system. Our expectation at the outset of the projects was that the combination of induction heating and thermography would outperform systems based exclusively on either electromagnetic induction or thermography. The rationale was that the combined system would offer better capabilities for wide area inspection of large structures than induction systems, and better sensitivity to deep, low aspect ratio indications than pulsed thermography. Ultimately, the results of the experiments in Task 4 did not entirely support our initial optimism. Although the proof-of-principal system did offer the anticipated advantages for wide area inspection, the sensitivity of the system did not exceed that of current pulsed thermography capabilities, and in fact, did not perform as well in some key respects. Although some aspects of the performance of the SIT system could perhaps be attributed to shortcomings in the design or construction of this first demonstration unit, analysis of the data indicates that some important limitations of the approach are fundamental.

The basic thrust of the experimental results can be summarized as follows: Although optical flash heating of the sample surface and induction heating of the sample bulk cause different thermal interactions with subsurface anomalies in carbon fiber composites, the effect of these interactions is communicated to the sample surface by thermal diffusion. Ultimately, the limitations imposed by the diffusion process are far more severe than those due to the heating process are. As a result, it appears that the ultimate sensitivity of the SIT approach is constrained by precisely the same considerations as the pure thermographic approach, namely, the aspect ratio of the subsurface defect. In other words, the sensitivity to fine structure (i.e. low aspect ratio features) that induction heating can provide at the defect plane is not resolvable at the sample surface plane, due to diffusion effects.

The details of the modeling and experimental tasks leading to this conclusion will be described in the subsequent sections.

Technical Background

Induction Heating of Carbon Fiber-Based Composites

Induction heating is a heating technology utilized for conductive materials including carbon fiber reinforced plastics for processes such as, bonding, curing and net-shape molding. Induction-based heat generation in carbon-fiber-reinforced composites occurs due to induced eddy currents flowing along global conductive loops in the composite, as shown in Figure 1. In each conductive loop, heating occurs wherever there is a voltage drop due to electrical impedance. The resultant heating is "volumetric" in nature with an internal heat generation mechanism dependent on intrinsic properties of the composite. Heating can occur either due to the fiber-based resistance network (in-plane and through-thickness) or due to dielectric hysteresis at the overlap junctions. Heat generation characteristics (pattern and rates) are dependent on 3-D carbon fiber network within the composite.

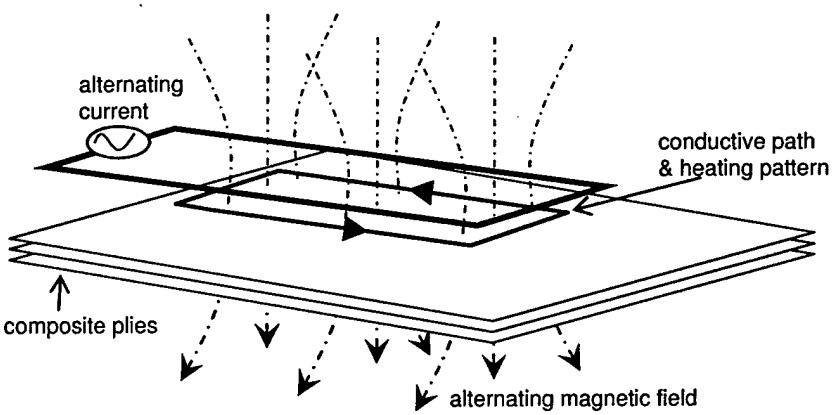

Figure 1. Schematic of the induction heating process of conductive fiber reinforced plies.

The major advantage of induction heating is the ability to achieve high volumetric heating rates, compared to conventional manufacturing processes that rely on conduction, convection, or radiation heat transfer through the thickness of composite. Volumetric heating leads to higher throughput and reduced cycle times; this is particularly advantageous for processing of thick-section composites. Many researchers have evaluated and developed induction-heating based systems for processing and fabrication of carbon fiber-based composites.

A unique feature of induction heating is the characteristic "edge effect". When the magnetic field from the induction coil is positioned near an edge of the composite, amplified heating occurs due to concentration of the magnetic flux lines near the edge, much like a stress concentration. Although this has been a common design problem for achieving uniform heating, it is a significant advantage where defect and crack detection is concerned. Since at any defect location, localized flux concentration will occur (similar to the free edge) resulting in higher relative heating. The degree of flux concentration is a function of the defect size and induction parameters and can be optimized to improve sensitivity and resolution. The same concept is used in eddy current sensors for defect detection in metal and carbon composite components, by measuring flux concentrations at defect locations. Due to the higher resistance, heat generation is a better metric for carbon fiber composites.

Pulsed Thermography

In active thermography, the front surface of a solid sample is heated either instantaneously or continuously while an IR camera monitors changes in the surface temperature. Surface areas located directly above subsurface flaws that obstruct the flow of heat into the sample will appear hotter than intact areas, which cool to equilibrium more rapidly. Near surface flaws with large aspect ratios may be detected using a simple heating apparatus (e.g. a hot-air gun or heat lamp) and visual observation of the camera video output. However, instantaneous heating, commonly referred to as Pulsed Thermography (PT), has become the preferred implementation of thermography in the aerospace, power generation and automotive industries, as it offers significantly better repeatability and sensitivity than continuous heating.

The implicit assumption in thermographic NDT is that after excitation of the sample surface, the primary mechanism for cooling of the surface is diffusion of heat from the surface into the sample bulk (i.e. radiation and convection cooling mechanisms may be ignored). In most inspection scenarios, this assumption is reasonable, and the diffusion process is well-represented by a 1-dimensional model, since lateral diffusion components cancel. However, the presence of a subsurface defect acts to obstruct this flow of heat from the surface into the cooler interior of the sample, so that subsequent cooling of the surface in the immediate area of the defect will be the result of incident heat flowing around the defect. In effect, detection schemes in pulsed thermography can be considered to be finding areas where normal cooling due to 1-dimensional diffusion has stopped, and other cooling mechanisms have taken over. This interaction is evident in the logarithmic surface temperature vs. time plot of sample response to an instantaneous heat pulse. The plot of the surface in a defect free area is essentially as straight line with slope -0.5, as predicted by the 1-dimensional diffusion equation. However, a subsurface defect causes a distinct deviation from linear behavior that occurs at a time that is correlated to the depth of the feature. This relationship has been exploited to allow detection and characterization of subsurface defects that are not detectable in the IR image produce by the camera. The time derivatives of this logarithmic time history are particularly sensitive to small anomalies in material properties.

Since thermal energy transport is a diffusion process, energy density decreases as propagation occurs. Thus, the amount of heat energy "trapped" between a defect and the surface decreases for deeper features, since more diffusion occurs during the transit time. In practical terms, this means that the size of the minimum resolvable defect is not a single number; it is a function of diameter and depth of the feature, where the minimum detectable defect size increases with depth. As a general rule of thumb, features with aspect ratio (diameter/depth) less than ~ 2 are extremely difficult to detect using thermography.

Objectives

The primary objective of this effort has been to demonstrate the feasibility of induction-heating based infrared thermography to detect various forms of damage in a carbon fiber reinforced composite using the inherent properties of the composite as the sensing mechanism. Several technical objectives must be met to demonstrate the feasibility of this approach:

- Establish the relationships between induction heating parameters and localized heating due to various types of damage and possible variations in manufacturing (fiber orientation, lay-up etc)
- Preliminary model development to enable prediction of expected induction heating pattern based on damaged carbon fiber resistance network
- Demonstrate damage detection using induction-coupled thermography
- Identify critical parameters to improve detection capability and resolution
- Address the limitations of numerical model in detecting defect/damage
- Assessment of hardware interfacing between induction heat generation and infrared thermography
- Cost, performance analysis and scale-up capability

The following sections document the numerical model description, model validation by experimental results, parametric studies and results, experimental results for variety of defects (holes, slits, delaminations), thermal imaging based on stationary and scanning methods.

Numerical Model

The objective of the numerical model is to predict heating behavior of a carbon fiber reinforced composite, given the induction parameters and composite configuration. This will enable model-based parametric studies to understand the influence of a defect on the 3-D carbon fiber based electrical network, predict expected changes in heating behavior due to defects and optimize parameters to maximize sensitivity. Materials considered in the model include both woven fabrics and unidirectional prepreg-based composites.

Overview/Heating Mechanisms

During induction heating, a carbon fiber reinforced composite can be separated into two distinct heat generation regions, within fibers and at fiber-fiber junctions (where fibers overlap). Fibers can generate heat due to their intrinsic resistance and junctions can generate heat due to either dielectric hysteresis heating if the fibers are separated by a small polymer gap or contact resistance heating if the fibers are in direct contact.

From a modeling aspect, the carbon fiber composite is idealized as a 3-D network with electrically conductive fibers and their junctions, with eddy currents flowing through the conductive network due to the applied alternating magnetic field. The heat generation methods are fiber Joule heating, fiber junction dielectric heating, and fiber junction contact resistance heating. The dominant type of fiber junction heating in the samples depends on the junction impedance/resistance, which is also dependent on processing conditions of temperature and compacting pressure.

Joule heating is the dominant mechanism for woven fabric laminate due to intimate contact between fibers (woven architecture) and high level of compaction. On the other hand, induction heating of unidirectional prepreg composite shows junction-heating dominance. The model used in this effort combines both heating mechanisms into a unified model.

Numerical Model Description

The numerical model is a 2-D lumped parameter approach that describes the 3-d conductive fiber network as a combination of lumped fiber grids and their junctions. A schematic of the meshing scheme is shown in Figure 2 below. The unit cell is a conductive electrical loop between two adjacent plies, with the fibers along the directions in each ply and the junction at the interface of the two plies. This methodology allows us to breakdown a lay-up sequence into a series of heat generating interfaces of layers, depending on which heat generation method is the dominant one. Initial studies were based on a simplified 2-ply composite construction, consequently heat transfer issues are not addressed in this effort.

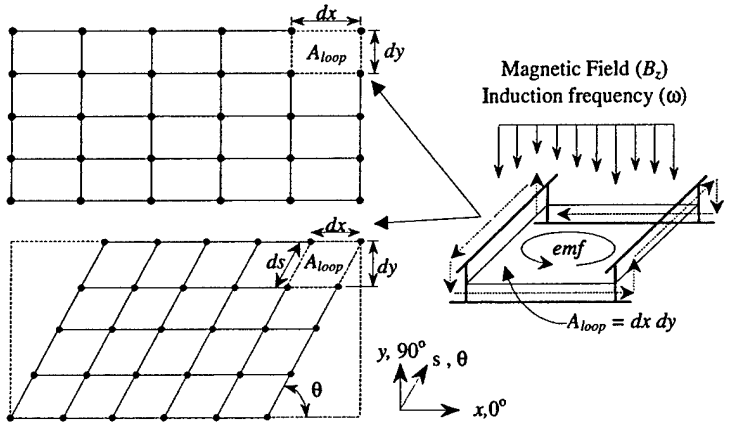

Figure 2. Numerical mesh scheme for cross-ply and angle-ply prepreg stacks.

The induction coil generates an alternating magnetic field, as it is a current carrying conductor, with a specified frequency. Biot-Savart's law is applied to the numerical mesh (nodal points) plane to calculate the magnetic field strength as a function of the coil geometry,distance between the coil and laminate and coil current. The field component perpendicular to the plane of the numerical mesh (or composite) is calculated and used to calculate the induced EMF currents in the conductive loop system. Voltage drops and currents across the fibers and junctions are calculated based on current conservation principles.

The numerical scheme is summarized in a flow chart, Fig. 3. A sparse matrix solver is used to handle the large number of unknowns and equations that arise from the current calculations over the mesh elements. For example, if we use a 100 x 100 mesh, there are 30401 unknowns, 30401 equations and 140800 non-zero terms in the 30410 x 30401 regular matrix.

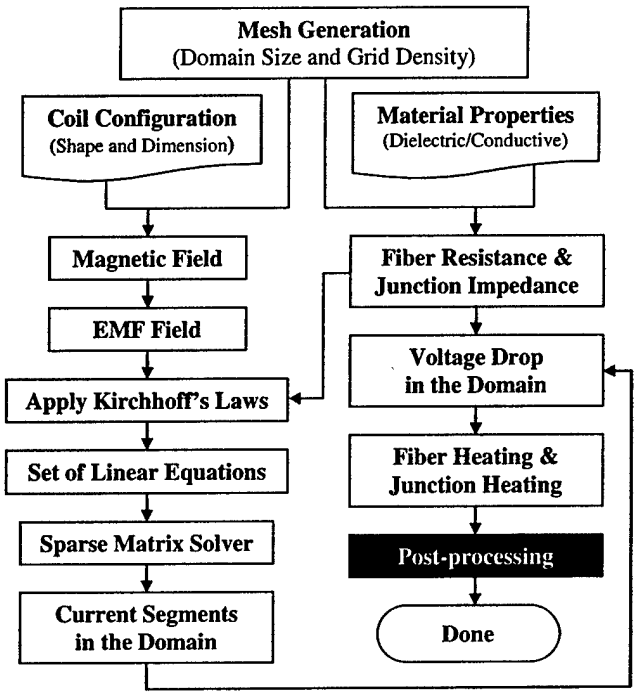

Figure 3. Flow chart of numerical model to predict heat generation.

Defects Treatment in Model

Defects in the composite typically result in either fiber breaks or delaminations and can be modeled as a combination of fiber or junction breaks in the electrical network described previously. In-plane fiber breaks are modeled as resistors with very high value, such that current flow is negligible. Delaminations can be modeled as junction breaks in the unit cell and in the case of woven fabrics may not significantly alter the heating pattern (will affect heat transfer). Larger defects can be modeled as areas with very high resistance in the fibers and junctions.

Processing Parameters

Parametric studies were performed using the model described above for the following relevant parameters: Induction frequency, Distance between coil and laminate, Coil shape and the dimension and finally the defect shape and the size

Experimental Description for Model Validation

Materials and Test Laminates

Two representative materials were chosen and laminates fabricated with and without defects. The first was a woven fabric laminate using T300/Cycom 970 prepreg from Cytec Fiberite. The laminate was fabricated using the manufacturer recommended procedure using an autoclave cure cycle at 350 F. Two model laminates were fabricated for numerical validation – a 1 layer laminate for In-plane defects (circular hole and rectangular hole) and a 2 layer laminate for through-thickness defect (delamination). The second material was a AS4/PEI unidirectional prepreg based laminate fabricated in a cross-ply configuration. Model laminates were fabricated from 3-plies in a [0/90/0] configuration for symmetry.

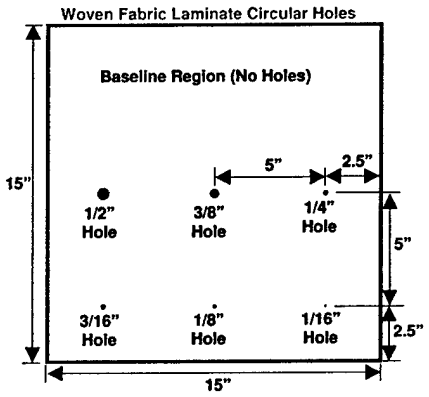

(a) Woven fabric laminate with circular through-holes

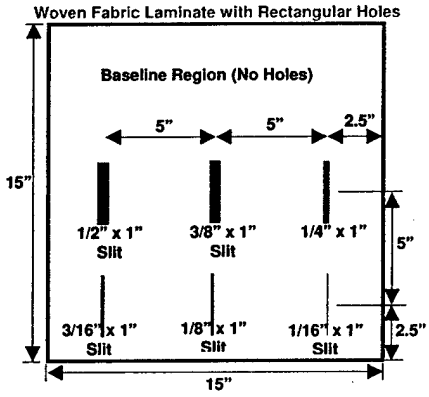

(b) Woven fabric laminate with rectangular through-holes

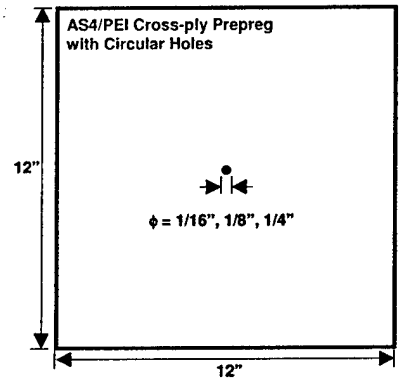

(c) Cross-ply laminate with circular through-holes

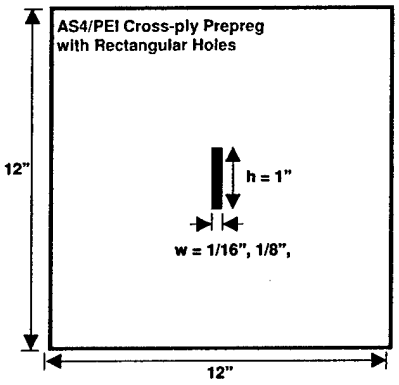

(d) Cross-ply laminate with rectangular through-holes

Figure 4. Test laminates with defects for comparison of numerical results with experimental data.

Model defect sizes were as follows for both materials and shown in Figure 4:

- Circular holes: 1/16", 1/8" and 1/4" in diameter
- Rectangular holes: 1/16", 1/8" and 1/4" x 1" (W x L)
- Delamination: 1/16", 1/8" and 1/4" x 1" (W x L, 3-mil Kapton tape)

Note that the 1/16" size is equivalent to a fiber tow width in the woven fabric composite.

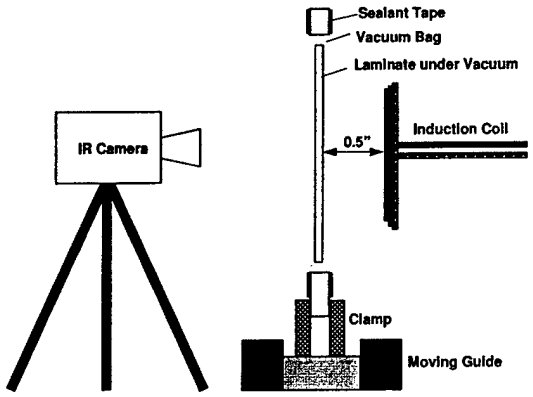

Figure 5. Schematic of the experimental setup

Model Validation Experimental Setup

The fabricated laminates were vacuum bagged in a frame to provide a flat and parallel surface to the induction coil. A bench top induction power supply manufactured by Hüttinger Electronic Gmbh, was used for the tests. It is rated for 5 kW maximum power output in a frequency range of 50 – 300 KHz range. This unit is a typical heating power supply and used for heating metals and other conductive materials to high temperatures. For our purposes, we expect to use very small power values in order to provide just enough heat to distinguish from the ambient temperature. For an actual NDE application, power levels may be as small as several hundred watts.

Both stationary and scanning heating experiments were performed for the test laminates. For the stationary tests, the laminates were positioned such that the center of the induction coil matched the position of the defect, Figure 5. For scanning experiments, laminates were moved vertically or horizontally at a constant rate. An AGEMA IR camera system was used to record thermal images during the experiments at a rate of approximately 3-4 frames per second. Two coil types were used in this study – a 4-turn pancake coil (in-plane spiral) and a butterfly coil (also known as a Double-D). The pancake coil was used for parametric studies and the butterfly coil, Figure 6, used for scanning experiment as this coil geometry generates a uniform strip of heat at the center of the coil. The domain size in the model was a 120 x 120 mesh for 8" x 8" domain on the laminate with 6.2" x 3.7" (W x L) butterfly coil. The test matrix for model validation experiments is shown in the Table 1.

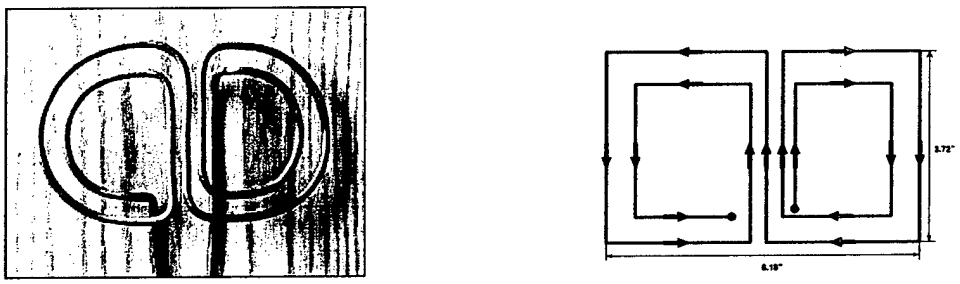

(a) Butterfly coil fabricated and experimentally used (b) Double 2-turn rectangular coil in numerical model

Figure 6. Double 2-turn rectangular coil to simulate a butterfly coil in the numerical model, and flow direction of electric currents.

Table 1. Test matrix on butterfly coil experiments

Laminate Type	Laminate Fabrication	Stationary or Moving	Damage Type	Damage Size	Image Session	Induction Parameters
Woven Fabric Laminate (1L, 9.5 mils) 18" x 16"	Autoclave 350F Cure for 0.5 Hours (under vacuum &85 psi) T300/Cycom970 from Cytec Multiple Damages in a Laminate	Stationary	Circular Hole	1/16" Diameter	HJ01	0.5 A 50.6 V 185.5 KHz
				1/8" Diameter	HJ02	
				1/4" Diameter	HJ03	
			Rectangular Hole	1/16" x 1" (W x L)	HJ04	
				1/8" x 1" (W x L)	HJ05	
				1/4" x 1" (W x L)	HJ06	
Woven Fabric (2L, 19 mils) 18" x 16"			Delamination	1/16" x 1" (W x L)	HJ07	0.6 A 38.8V 182.5 KHz
				1/8" x 1" (W x L)	HJ08	
				1/4" x 1" (W x L)	HJ09	
Woven Fabric (1L, 9.5 mils) 18" x 16"		Moving	Circular Hole	1/16" Diameter	HJ10	0.5 A 50.6 V 185.5 KHz
				1/8" Diameter	HJ11	
				1/4" Diameter	HJ12	
			Rectangular Hole	1/16" x 1" (W x L)	HJ13	
				1/8" x 1" (W x L)	HJ14	
				1/4" x 1" (W x L)	HJ15	
Woven Fabric (2L, 19 mils) 18" x 16"			Delamination	1/16" x 1" (W x L)	HJ16	0.6 A 38.8V 182.5 KHz
				1/8" x 1" (W x L)	HJ17	
				1/4" x 1" (W x L)	HJ18	
Cross-ply Laminate (3L, 20 mils) 12" x 12"	Autoclave 600F Cure for 0.5 Hours (under vacuum & 85 psi) AS4/PEI from Cytec Single Damage in a Laminate	Stationary	Circular Hole	1/16" Diameter	HJ19	0.8 A 71.9 V 175.2 KHz
				1/8" Diameter	HJ20	
				1/4" Diameter	HJ21	
			Rectangular Hole	1/16" x 1" (W x L)	HJ22	
				1/8" x 1" (W x L)	HJ23	
				1/4" x 1" (W x L)	HJ24	
			Delamination	1/16" x 1" (W x L)	HJ25	
				1/8" x 1" (W x L)	HJ26	
				1/4" x 1" (W x L)	HJ27	
		Moving	Circular Hole	1/16" Diameter	HJ28	
				1/8" Diameter	HJ29	
				1/4" Diameter	HJ30	
			Rectangular Hole	1/16" x 1" (W x L)	HJ31	
				1/8" x 1" (W x L)	HJ32	
				1/4" x 1" (W x L)	HJ33	
			Delamination	1/16" x 1" (W x L)	HJ34	
				1/8" x 1" (W x L)	HJ35	
				1/4" x 1" (W x L)	HJ36	

Validation Experiment Results

Model predictions were validated using qualitative comparisons between the temperature distribution from thermography and heat generation from numerical results at short time scale to reduce in-plane heat diffusion. Due to the larger coil size, edge heating effects are expected in some heating patterns. Circular holes in woven fabric and cross-ply laminates were considered for validation

Woven Fabric Laminate

Very good agreement is seen in Figure 7 between experimental and numerical results in the heating patterns for both baseline laminate and defective laminate. A 1" x 4" uniform heating zone occurs at the center of the coil which is expected based on the design of the coil. Similar results were obtained for smaller hole sizes (up to 1/16" hole).

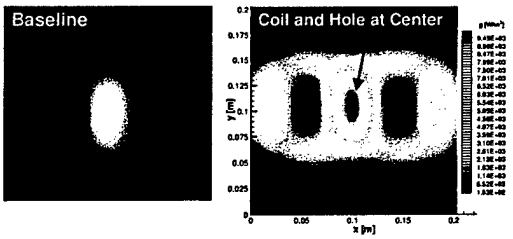

(a) Baseline (no defects)

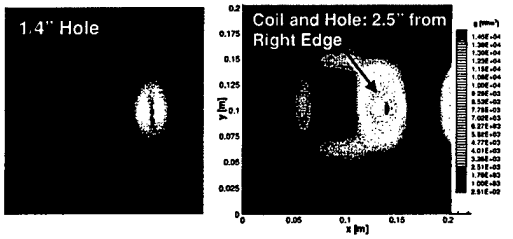

(b) 1/4" circular hole located 2.5" from the right edge of the coil

Figure 7. Comparison of experimental and numerical heating patterns for a baseline laminate and a defective laminate with 1/4" hole in woven fabric laminate (butterfly coil).

Cross-ply Laminate

Agreement in the cross ply laminate, Figure 8, is reasonably good, though we do not see the heat amplification or hot spots around the hole. This is a limitation of the numerical mesh size as we need to use a smaller representative cell size for unidirectional prepregs, as there are no fiber bundles. Using a fiber mesh around the hole can provide better results and this aspect will be explored in the next phase. However, cold lines due to broken electric paths are clearly detectable as well as hot spots in experiment.

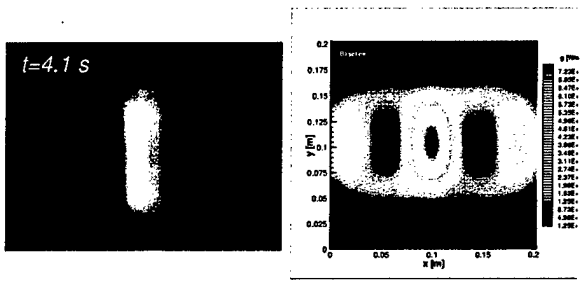

(a) Baseline (no defects)

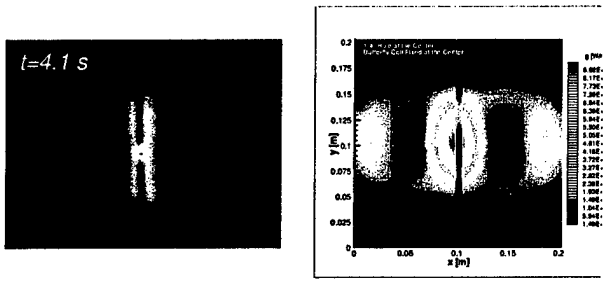

(b) 1/4" circular hole

Figure 8. Comparison of experimental and numerical results with different size of circular holes in cross-ply laminate for butterfly coil.

Parametric Study Reults

To improve sensitivity and contrast, a parametric study was conducted using a reference 4-turn pancake coil. The major parameters considered were

- Induction frequency (*f*)
- Distance between the coil and laminate (*d*)
- Scan Sensitivity Study on Thermal Contrast
- Coil shape and the dimension
- Defect type and the size

Induction Frequency

During induction heating, *EMF* generation is proportional to the frequency of the magnetic field. Assuming that the conductivity is independent of frequency in carbon fiber-based composites, no qualitative changes in heating patterns and thermal contrast with frequency were noted. There is an overall decrease/increase of heat generation depending on whether the frequency decreases or increases, but the thermal contrast remains the same, Table 2.

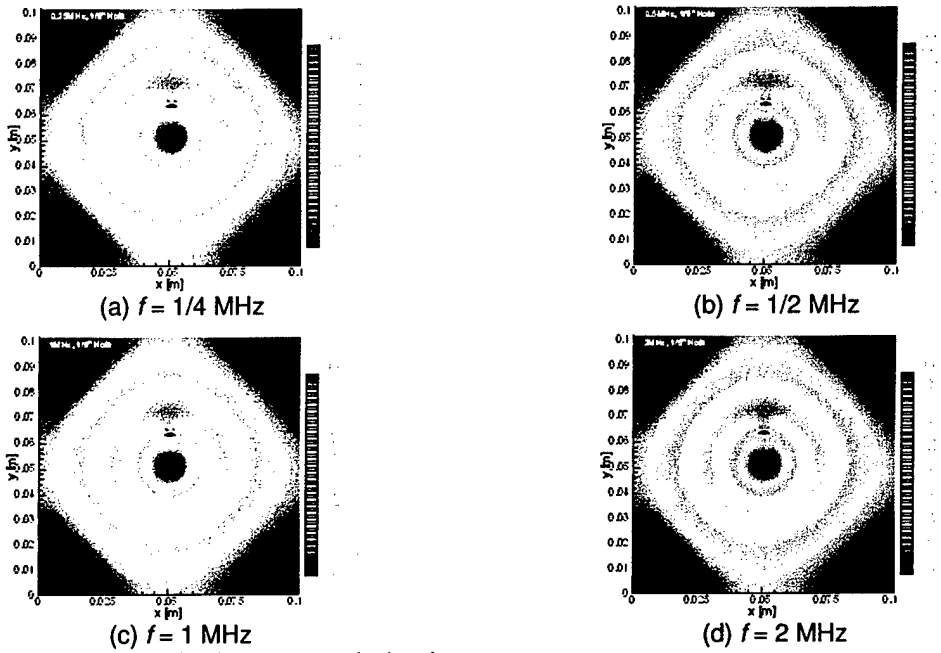

(a) f = 1/4 MHz (b) f = 1/2 MHz

(c) f = 1 MHz (d) f = 2 MHz

Figure 9. Effect of induction frequency on the heating patterns.

Table 2. Maximum heating, minimum heating and thermal contrast around the defect with varying induction frequency.

Freq. f (MHz)	Maximum Heating around the defect			Minimum Heating around the defect			Thermal Contrast around the defect	
	x (mm)	y (mm)	Heating Intensity (g_{max}, W/m^3)	x (mm)	y (mm)	Heating Intensity (g_{min}, W/m^3)	g_{max} / g_{min}	Normalized (based on g_{max} / g_{min} at 1MHz)
0.25	49.2	65.3	2.89×10^{4}	50.8	63.5	1.55×10^{-5}	1.87×10^{9}	1
0.5			1.16×10^{5}			6.20×10^{-5}	1.87×10^{9}	1
1			4.63×10^{5}			2.48×10^{-4}	1.87×10^{9}	1
2			1.85×10^{6}			9.92×10^{-4}	1.87×10^{9}	1

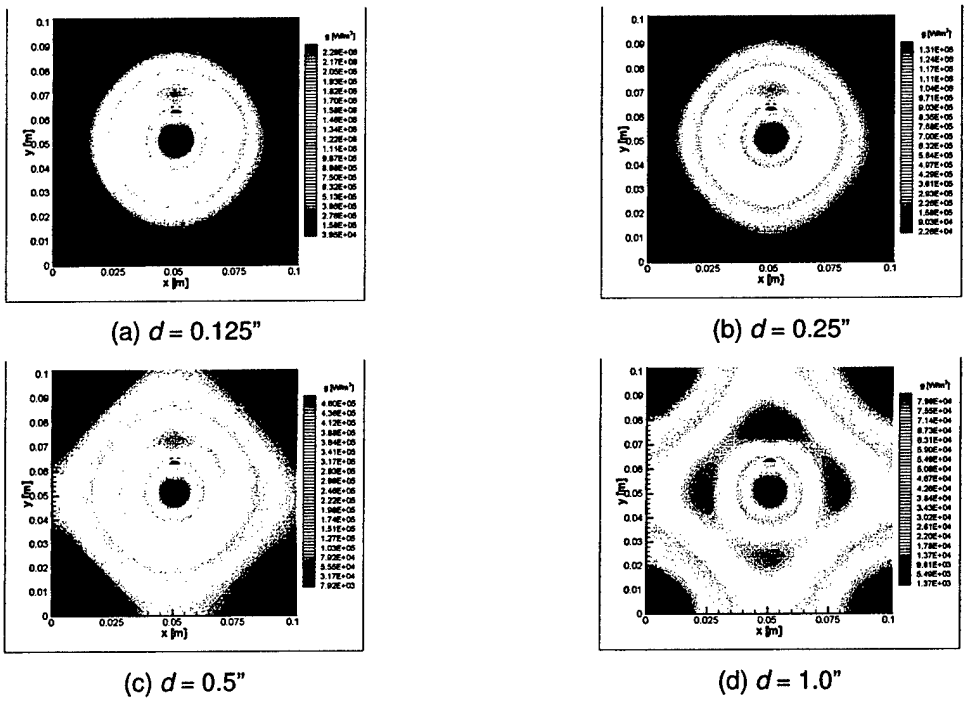

(a) $d = 0.125$" (b) $d = 0.25$"

(c) $d = 0.5$" (d) $d = 1.0$"

Figure 10. Effect of coil-to-laminate distance on the heating patterns.

Effect of distance between coil and laminate

In general, closer proximity should enhance thermal contrast somewhat, as that increases the field strengths and reduces the "smoothing" effect that we see with increasing distance. Predictions from the model show a small increase in thermal contrast when the coil is closer to the laminate – 7% increase in contrast from 1 inch spacing to 1/8" spacing. This can lead to a two-phase scanning method, where a global scan is performed at a larger distance from the part and a finer local scan with closer proximity.

Table 3. Maximum heating, minimum heating and thermal contrast around the defect with varying distance.

Coil to Laminate distance (in)	Maximum Heating around the defect			Minimum Heating around the defect			Thermal Contrast around the defect	
	x (mm)	y (mm)	Heating Intensity (g_{max}, W/m^3)	x (mm)	y (mm)	Heating Intensity (g_{min}, W/m^3)	g_{max} / g_{min}	Normalized (based on g_{max} / g_{min} at 1MHz)
0.125	49.2	65.3	2.31×10^6	50.8	63.5	1.16×10^{-3}	1.99×10^9	1.07
0.25			1.32×10^6			6.89×10^{-4}	1.92×10^9	1.03
0.5			4.63×10^5			2.48×10^{-4}	1.87×10^9	1
1.0			7.16×10^4			3.85×10^{-5}	1.86×10^6	0.99

Defect Size and Location Effect on Thermal Contrast

For a fixed coil location, the location of the defect in the composite affects thermal contrast, which makes moving scans necessary. The Figure below shows predicted maximum heating or thermal contrast as a function of defect location (a hole in this case) with respect to the coil. For all cases, there is an optimal scan location that provides maximum thermal contrast. A decreased in hole size causes lower thermal contrast as this due to the smaller effect on electrical network in composite, and the resultant smaller effect on the heat generation pattern that can be detected. Note that the infrared images shown are for short-time span temperatures to minimize diffusion effects, such that comparison with heat generation predictions from the model is possible. We expect that image processing will be required to magnify effect of smaller holes (less than 1/16") in the composite.

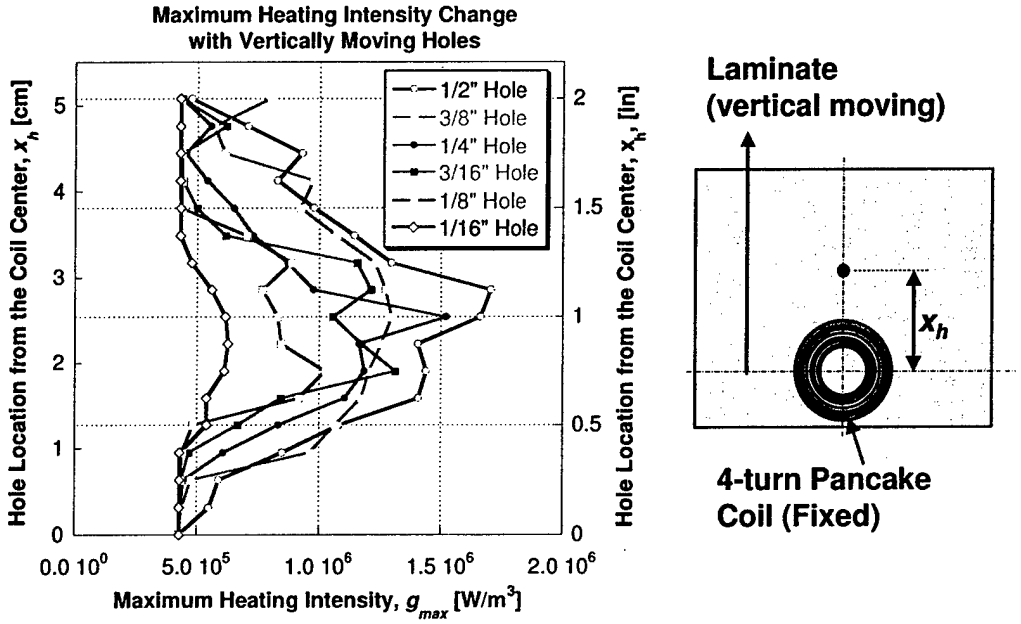

Figure 11. Thermal contrast (relative heating rate intensity) with defect size and the location.

Effect of Defect Size and Geometry

Circular Holes in Woven Fabric Laminate

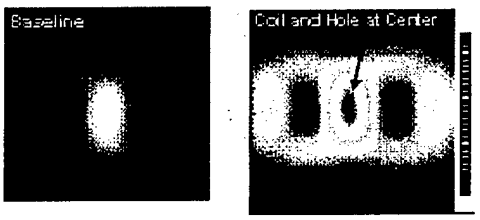

(a) Baseline (no defects)

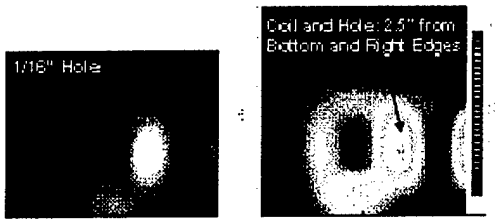

(b) 1/16" circular hole located 2.5" from the bottom and right edges of the laminate

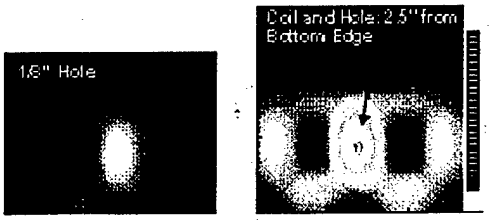

(c) 1/8" circular hole located 2.5" from the bottom edge of the laminate

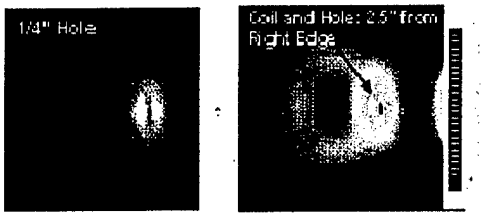

(d) 1/4" circular hole located 2.5" from the right edge of the coil

Figure 12 Comparison of experimental and numerical results with different size of circular holes in woven fabric laminate for butterfly coil.

Circular Holes in Cross-ply Laminate

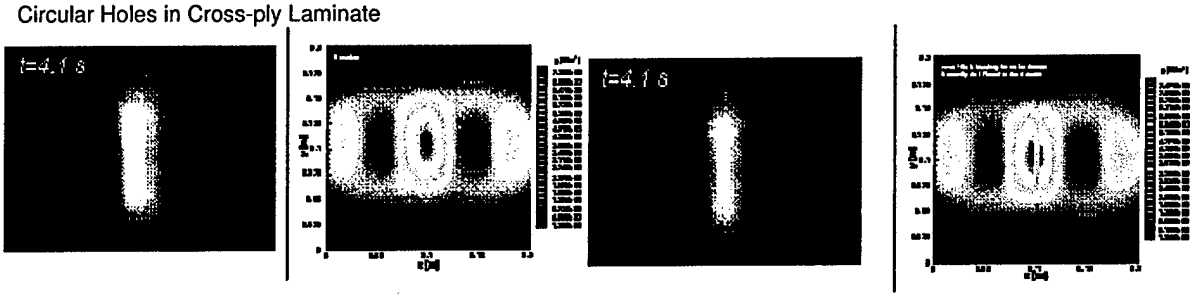

(a) Baseline (no defects)

(b) 1/16" circular hole

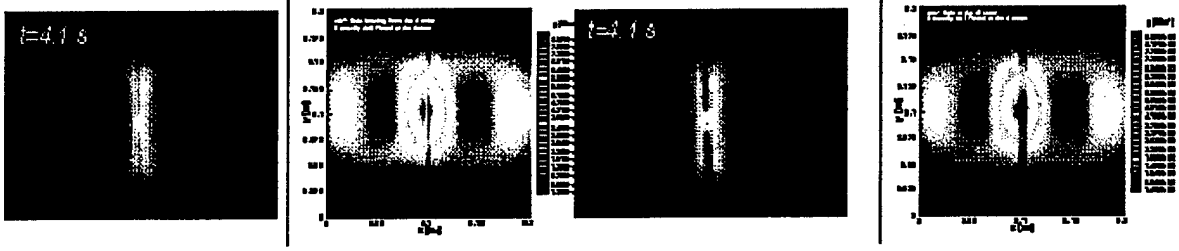

(c) 1/8" circular hole

(d) 1/4" circular hole

Figure 13. Comparison of experimental and numerical results with different size of circular holes in cross-ply laminate for butterfly coil.

Rectangular Slits in Woven Fabric Laminate

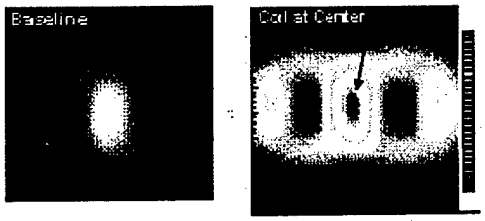

(a) Baseline (no defects)

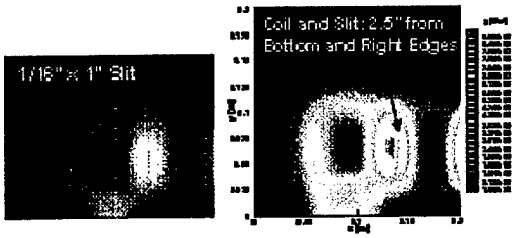

(b) 1/16" rectangular hole located 2.5" from the bottom and right edges of the laminate

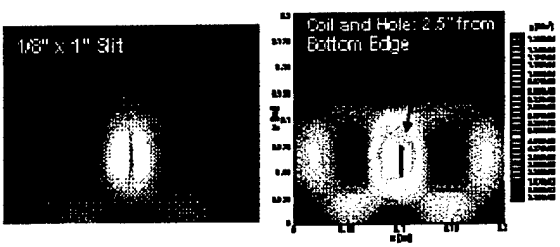

(c) 1/8" rectangular hole located 2.5" from the bottom edge of the laminate

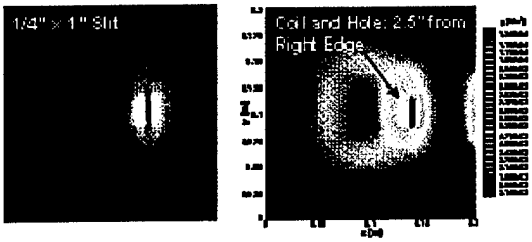

(d) 1/4" rectangular hole located 2.5" from the right edge of the coil

Figure 14. Comparison of experimental and numerical results with different size of rectangular holes in woven fabric laminate for butterfly coil.

Rectangular Slits in Cross-ply Laminate

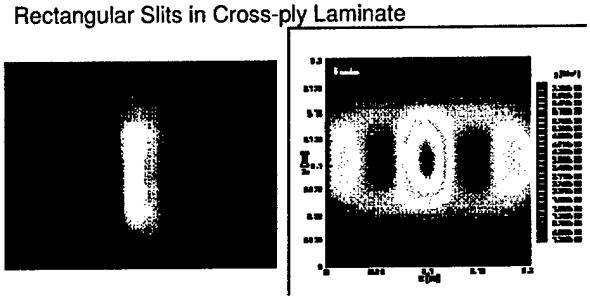

(a) Baseline (no defects)

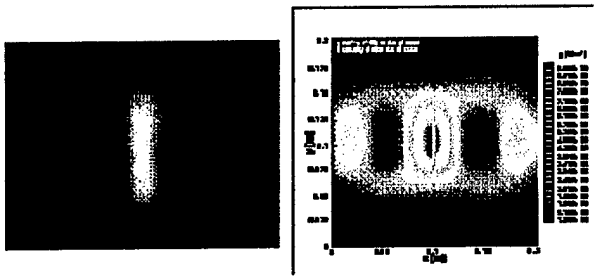

(b) 1/16" rectangular hole

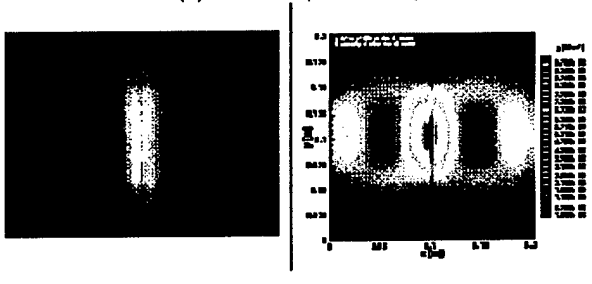

(c) 1/8" rectangular hole

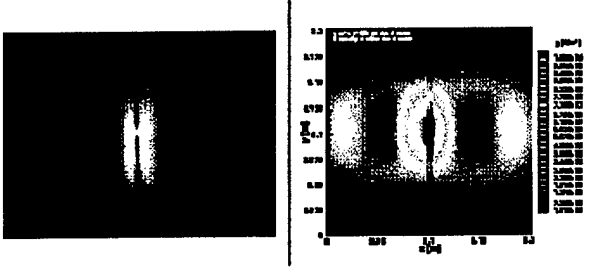

(d) 1/4" rectangular hole

Figure 15. Comparison of experimental and numerical results with different size of rectangular holes in cross-ply laminate for butterfly coil.

Delamination in Woven Fabric Laminate

One layer of Kapton tape was used between the two layers of woven fabric prepreg prior to autoclaving in order to simulate delamination. The IR images give somewhat blurred thermal contrast due to increased in-plane heat dissipation in each prepreg layer causing reduced or slow through-thickness heat transfer through the Kapton tape. For woven fabric prepregs, height information could be inferred from the IR images where two hot strips at the edges of the delamination. For cross-ply laminates, however, both the width and height information was available from the IR images.

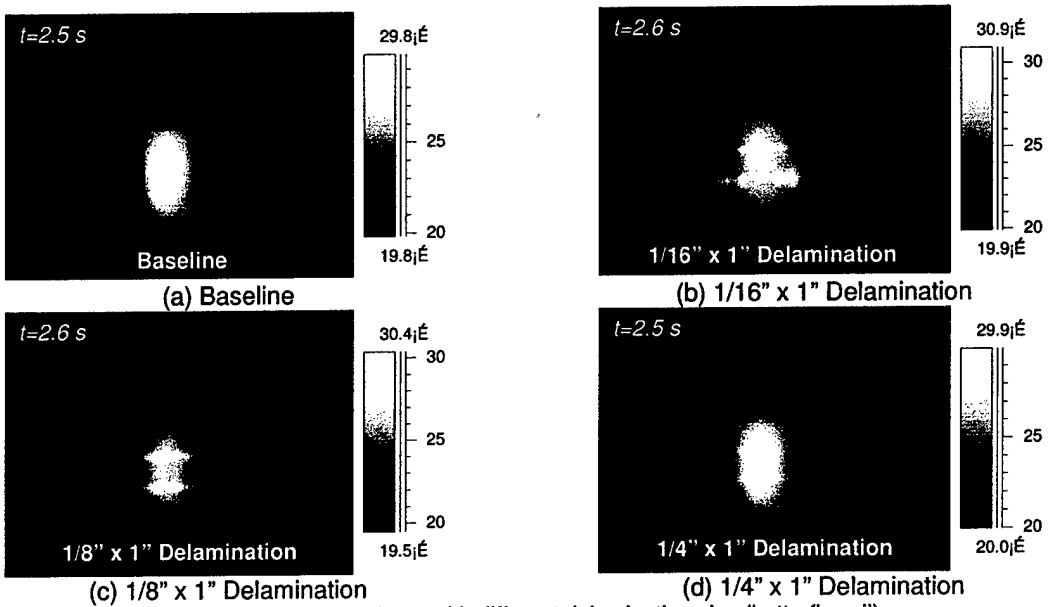

Figure 16. IR images of woven fabric laminate with different delamination size (butterfly coil).

Delamination in Cross-ply Laminate

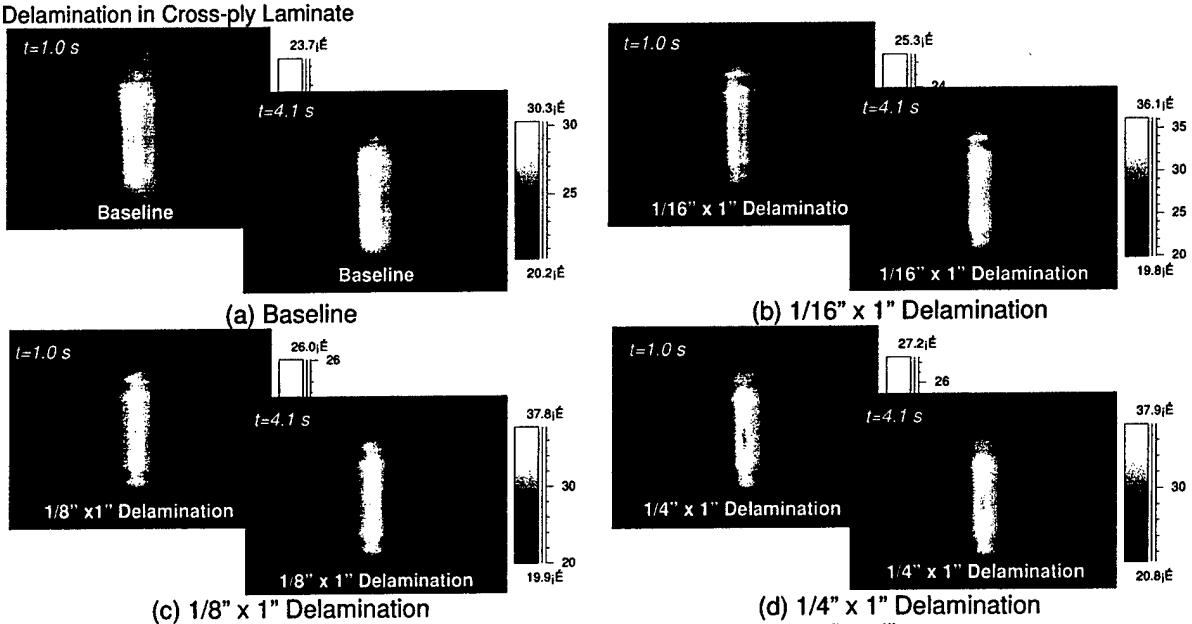

Figure 17. IR images of cross-ply laminate with different delamination size (butterfly coil).

Modeling Summary

A previously developed numerical model for prediction of heat generation in carbon fiber composites was modified to address the presence of defects in the laminate. The carbon fiber composite was simulated as a network of electrical elements, which generate currents in the presence of an alternating magnetic field. Defects were simulated either as fiber breaks (elements with very high resistance) or as junction breaks (layer to layer) in the case of delaminations. The presence of a defect in the laminate causes localized heating around its perimeter due to increased concentration of flux lines – the enhanced thermal contrast clearly enables detection of the defect. This was validated through model-experiments that showed good correlation between the model predictions and short time-scale heating patterns of both woven and unidirectional prepreg based composite laminates. For the evaluated representative composite materials, the smallest hole size detectable was 1/16" (which also corresponds to one fiber tow width of the fabric) using a standard IR camera system. Smaller defects will require either image analysis to improve thermal contrast or higher resolution camera systems. A parametric study of induction parameters showed that smaller gap between coil and composite is preferable, with a trade-off with field of view and surface curvature of part. The induction coil used affects the field distribution and thermal response of the composite and a uniform field generating coil design is preferable when scanning is required. Higher frequency does not affect thermal contrast, however, frequency affects skin depth, which affects heat generation through the thickness of the composite. This may be exploited to selectively heat a specific thickness of the composite (thickness-based scanning).

Experimental Evaluation of Scanning Induction Thermography (SIT)

Pulsed thermography, using flashlamps to heat the surface, is widely used for nondestructive inspection of composites. The technique is effective for finding delaminations, porosity or inclusions, but limited in the ability to detect subsurface features where the diameter is less than the depth. A similar scheme, but based on depositing heat in the sample using induction heating, rather than on the surface, offers the potential of significantly improved sensitivity for low-aspect ratio features. Since an RF-induction coil generates current loops in a carbon-fiber composite sample, and an IR camera can detect changes in the sample surface temperature, it is a relatively simple matter to confirm that induction does cause heating of the sample. However, there are several considerations that make an actual inspection device based on this principle more complicated:

- Although the magnitude of the local surface temperature field in the vicinity of the coil may be large with respect to the normal dynamic range of the camera, anomalies due to defects may be small and localized, and consequently, difficult to detect against the backdrop of the elevated background temperature
- Modeling shows significant temperature changes at material discontinuities. However, in the case of subsurface defects the effect of these changes diffuses to the surface, where the IR temperature measurement is made. Thus, a localized temperature increase beneath the surface will spread as it reaches the surface and may be undetectable with an IR measurement.
- Features on the surface as well as those located throughout the sample volume are likely to have some thermal response to induction heating, leading to possible false indications.

A proof of concept SIT device was developed and constructed to evaluate the feasibility of scanning actual carbon fiber composite components using induction heating. For the purposes of the Phase I program, only flat samples with relatively high IR emissivities were considered. Samples were also evaluated using a commercial Pulsed Thermography system, in order to compare the relative merits of the scanned approach

Synchronized Scanning

A proof of concept Scanning Induction Thermography (SIT) system was constructed in Phase I. In the basic (unsynchronized) single sided scanning configuration, data is acquired while the sample moves with respect to the camera and coil (Figure 16). The camera is positioned so that the field of view includes the portions of the sample on both sides of the coil, i.e. before and after a given line of interest moves directly under the coil (preheating data is required for subsequent processing operations, where temperature rise above the local ambient temperature is required). The presence of the coil in the field of view obstructs the sight line of the camera to those pixels directly under the coil. The geometry of the coil, a paper clip configuration with the loop perpendicular to the sample surface, was chosen to minimize the obstruction, and maximize the viewable surface area. The coil was placed in close proximity (~ 0.125") from the sample surface.

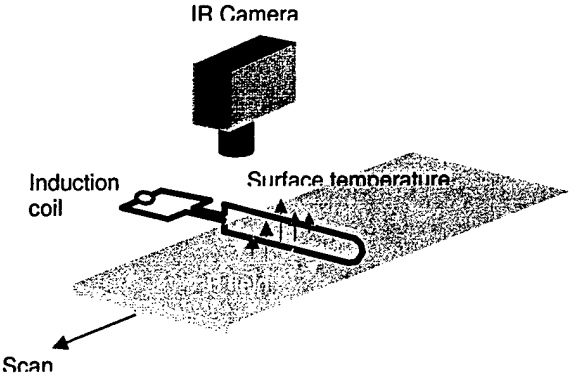

Figure 16. Basic SIT setup (single side). The camera and induction coil are held in fixed positions while the sample is translated across the field of view.

The scanning rate is dependent on the nature of the inspection to be performed. The propagation time for the electromagnetic energy from the coil is instantaneous, compared to the much slower diffusion process that carries the subsurface temperature distribution to the sample surface, and it is the slower process that determines the scan time. Thus, for detection of surface breaking features (e.g. cracks or holes) diffusion plays a minimal role, so the scan speed can be quite fast, i.e. limited only by the camera frame rate and the desired spatial resolution (the camera speed should not exceed one spatial resolution element per frame). However, the objective of this study is to detect subsurface features, where the time scale of the contrast generation mechanism is entirely based on diffusion. The appropriate scan speed for the CFRP flat bottom hole test sample was estimated using pulsed thermography data, where the peak contrast time (PCT) for a feature with diameter D and depth d can be estimated as

$$PCT = \sqrt{2\pi}Dd\,.$$

Using the equation above as a guideline, we require that a point on the surface remain in the field of view for a duration equal to or greater than the peak contrast time. In fact, this is a very conservative criterion, since:

a) In pulsed thermography, thermal energy must diffuse form the surface to the defect plane, and then the effect of the interaction at the defect plane must diffuse back to the surface. However, induction heating is virtually instantaneous, so only the defect to surface diffusion is involved.

b) In subsequent processing, we will look at time derivatives of the surface temperature that occur before the peak contrast time.

In the unsynchronized mode, the system is only useful for viewing the response of a rectangular stripe of the sample surface (perpendicular to the scan direction) just after it passes under the coil, i.e. it is not possible to view the response of the entire sample in a single image (Fig. 17). Although features on the surface (e.g. the surface texture) are well resolved, indications of subsurface features detected in the raw mode are blurry, and potentially difficult to interpret, as stripes at different distances from the heating coil have entirely different time histories.

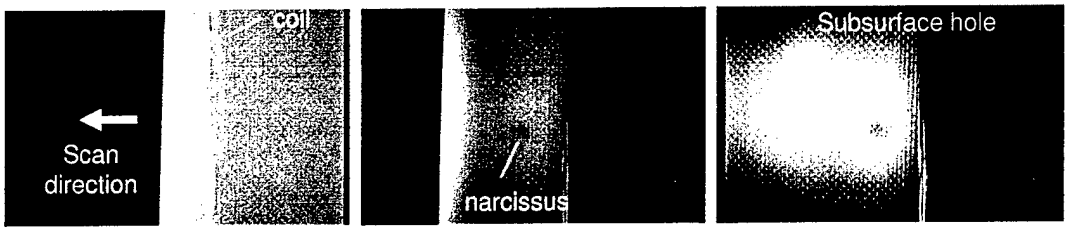

Figure 17. Raw images from scan of the CFRP flat bottom hole target. The coil and the reflected image of the cooled detector (narcissus) remain fixed as the sample moves to the left. A weak indication of a 0.75 in diameter subsurface hole is seen in the rightmost image.

Synchronized Scanning and Scan Reconstruction

Precise synchronization of the camera frame acquisition to the translation of the camera relative to the sample allowed us to independently analyze and process the temperature response of each point on the sample surface, in order to optimize sensitivity. For the purposes of analysis and processing, the acquired data must be converted to a format where the acquired data sequence appears to be stationary in space. In other words, the actual data recorded by the camera shows a moving panel, while the converted data will represent an equivalent stationary panel. In order to do this, the motion of the camera must be synchronized to the motion of an instantaneous field of view of a single pixel in the camera focal plane, such that with each frame, the sample moves a distance exactly equivalent to a single pixel field of view (Figure 18).

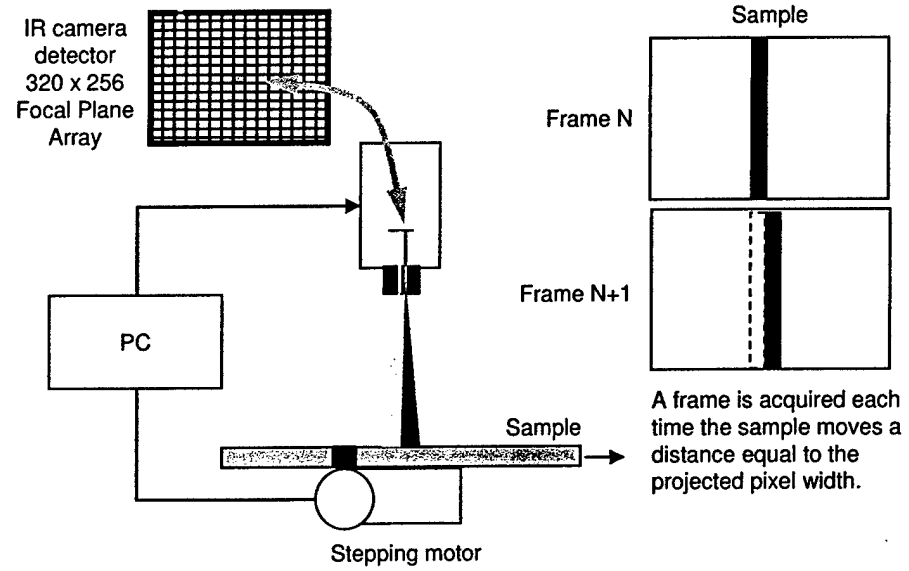

Figure 18. Synchronized scanning. The sample moves a distance equivalent to the distance between pixels that have been projected onto the sample.

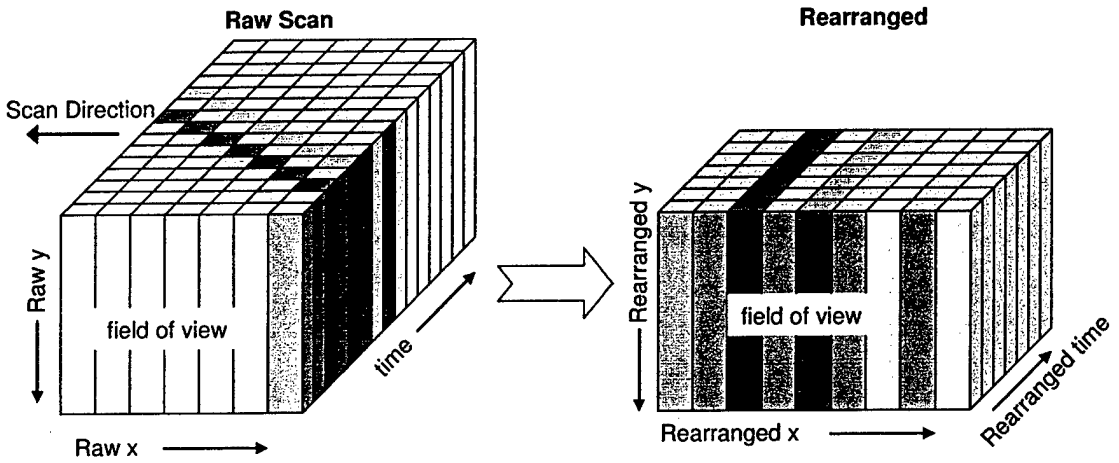

Figure 19. Rearrangement of the synchronized data sequence.. In the raw sequence (left), a stripe on the sample appears to move in the scan direction over time. Rearrangement of the data creates a data sequence of a target that appears to be stationary.

Once the data from the synchronized scan has been acquired, it is rearranged so that the stripe on the surface appears to be stationary. The rearrangement process treats each column in a single image as temporally coherent, where time is taken to be relative to the passing of a point directly under the coil. Individual columns that have passed under the coil represent the state of the sample at progressively later times (a column close to the coil has just been heated, while a more distant column was heated at an earlier time). In the rearranged sequence, columns are interchanged so that temporal coherence of the column is preserved through throughout the sequence (Fig. 19). In the rearranged sequence, the y dimension of the image is determined by the camera focal plane, while the x dimension is determined by the duration of the scan, regardless of the focal plane dimensions. In Fig. 20, the FBH test sample is scanned with a 320 x 252 active pixel focal plane, yielding a reconstructed image with dimensions 640 x 252 pixels.

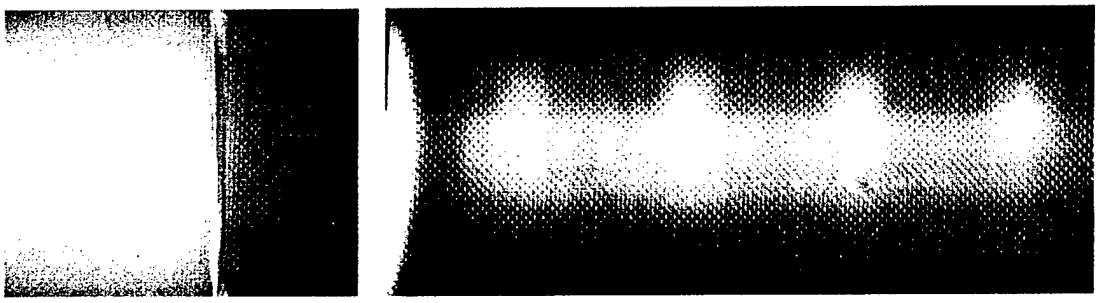

Figure 20. Images from the raw scan sequence (left) have the dimensions of the camera focal plane (320 x 252). In the rearranged data, the x-dimension depend on the duration of the scan, and the image dimensions are 640 x 252.

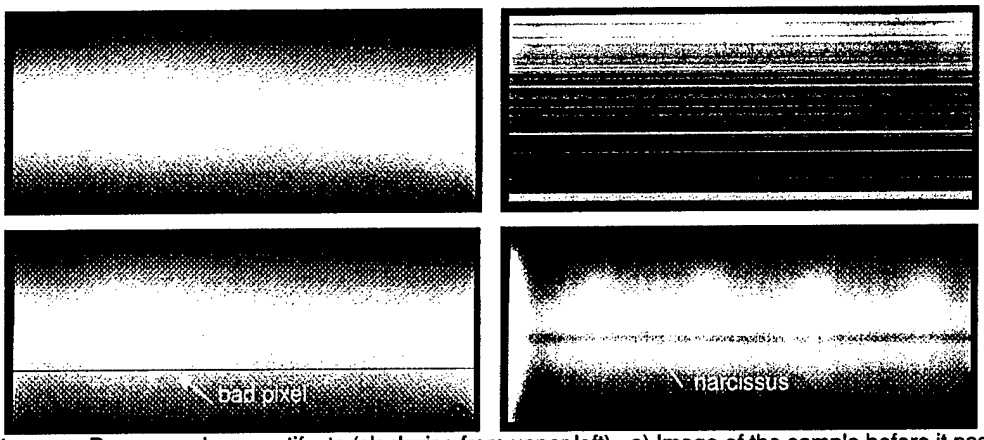

Figure 21. Rearranged scan artifacts (clockwise from upper left). a) Image of the sample before it passes under the induction coil; b) Image during coil passage blind interval; c) transient image of narcissus; d) transient image of a bad pixel.

The rearranged image sequence appears stationary, so that the time evolution of a single pixel represents the temperature history of a particular point on the sample. This process of deconvolving the actual motion of the part to create an apparently stationary image affects several characteristics of the sequence. In particular, image features or artifacts in the original sequence that appear to be stationary in will appear as transient events in the rearranged sequence. For example, the induction coil is a vertical stripe in the raw sequence located near the center of the field of view. The coil blocks the camera sight line to the sample, the sample area directly under the coil is not visible. In the rearranged image sequence, the passage of a point on the sample under the coil is a distinct event in time, and during that time, the point under consideration is obscured. As a result, spatially discrete artifacts such as a single bad pixel, or narcissus (self-imaging of the detector) appear as transient lines or stripes that are parallel to the scan direction (Fig. 21). Such events cause the time history of particular pixels to be discontinuous, and in the case of the coil passage, which affects all pixels, a blind interval will occur in which all pixels are temporarily obscured (Fig. 22).

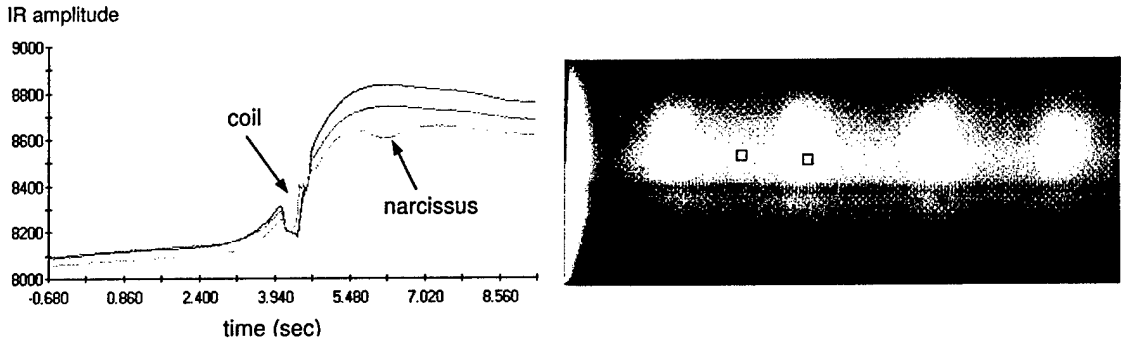

Figure 22. Effect of scan artifacts on pixel time history. A discontinuity occurs in the time history of all pixels as the coil obstructs the camera sightline. However, stationary artifacts such as the self-reflection of the camera appear as transient effects in the time history.

The rearrangement process also changes the noise characteristics of the sequence. In the normal sequence, in the original sequence the primary intrinsic noise sources are temporal noise from the camera electronics, and fixed pattern spatial noise from the camera focal plane. The time varying noise is random, and is distributed evenly over the rearranged sequence. However, the stationary fixed pattern noise becomes a moving noise source in the rearranged image, with apparent motion in the scan direction. The fixed pattern (nonuniformity) noise is a well-know and inherent property of focal plane detectors, and a consequence of the fact that the focal plane detector comprises

over 80,000 discrete detector elements, each with its own gain and offset characteristics, so that truly uniform response is essentially impossible to achieve.

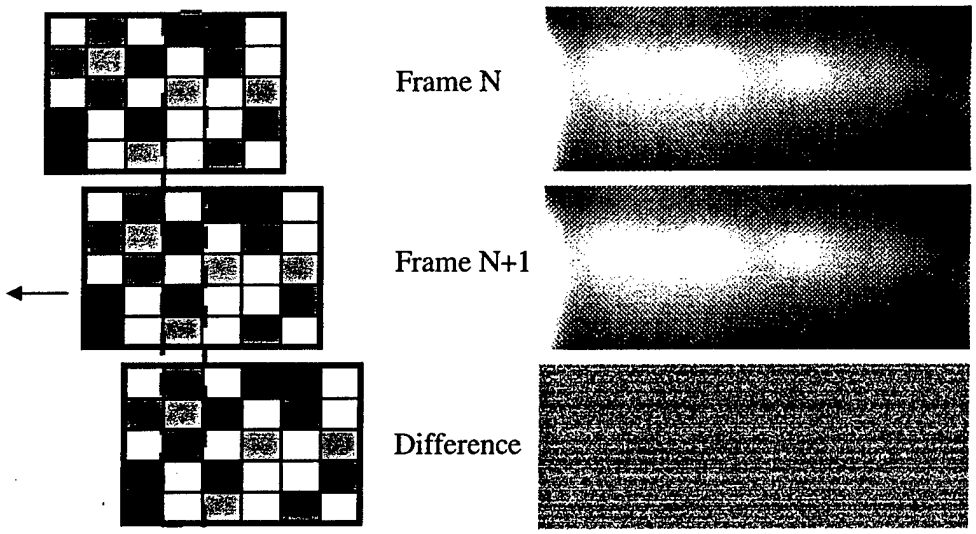

Figure 23. Fixed pattern noise artifacts. Left: Synchronized translation of the sample relative to the camera results in moving the fixed noise pattern by one column with each frame. Right: Subtraction of adjacent images in the sequence leaves only the difference in the two columns' noise patterns, extended over the entire image.

Signal Processing

Several signal processing strategies were applied to the rearranged data in order to reduce noise, remove artifacts, and improve detectability of subsurface features. The simplest method applied was background subtraction, in which a rearranged image of the sample before heating by the coil was subtracted from all images after heating. The preheat image was constructed from a column on the sample where a small amount of heating is just beginning to occur, so that artifacts such as reflected radiation from the coil, or nonuniform heating along the coil direction are included. Background subtraction does offer some degree of target-contrast improvement for subsurface features (Fig. 24). However, it also improves resolution of features on the surface, which may obscure more subtle subsurface features.

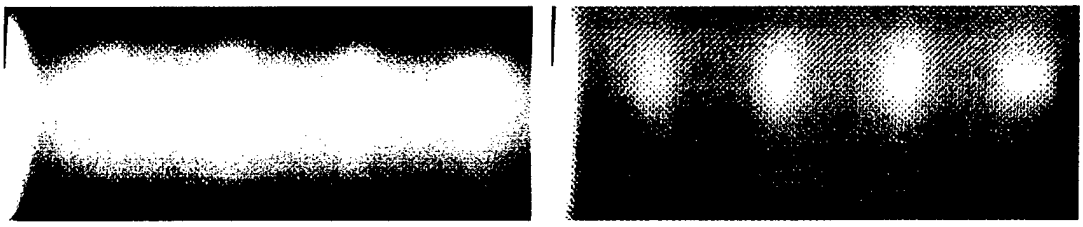

Figure 24. Background subtraction. Left: Rearranged image after induction heating. Right: Same image after background subtraction. The shape of the four subsurface holes is more distinct, and the surface texture of the sample is apparent in the background-subtracted image.

A more complex signal processing approach involving reconstruction of the entire time history of each pixel was also implemented. This Scan Reconstruction approach was modified version of the Thermographic Signal Reconstruction method that is widely used to great advantage in pulsed thermography. The method takes advantage of the fact that thermographic time sequences that depend on heat conduction into the sample as a primary cooling mechanism are

predictably slow and smooth, with shapes that are highly deterministic for defect free samples. Thus, the time history of each pixel can be accurately represented by an approximation that can be a series expansion, or a basis set of orthogonal functions. The resulting representation relatively free of temporal noise, and it is readily differentiable, so that time derivative images can be constructed to represent any time in the sequence. In pulsed thermography, the time derivative images are far more sensitive to subsurface features than the original temperature images.

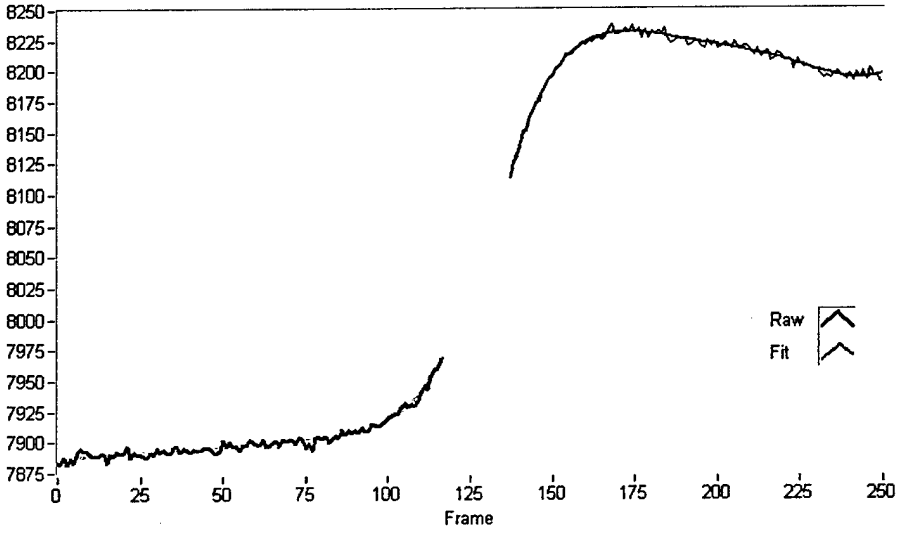

Figure 25. Polynomial fit of rearranged scan data. The reconstructed time history (red line) based on a 6th order polynomial fit of the raw data (black line) is relatively free of temporal noise. The gap in the middle of the sequence is due to the passage of the induction coil.

For SIT data, the situation was complicated by the interruption of all pixel time histories by the scanning coil. The coil discontinuity requires that each pixel be treated as having separate pre and posting heating time histories, which would be approximated separately. Both segments were fit to a 6th order polynomial using a least squares approximation, with a gap in the data during the coil passage interval.

The effect of the polynomial reconstruction on noise is not obvious in comparing single images. However, in viewing reconstructed sequences as movies, one observes that the moving focal plane fixed pattern noise is entirely removed. This can be demonstrated by viewing the difference between images representing consecutive frames (Fig. 26), where the polynomial reconstruction difference image is free of fixed pattern artifacts, and contains only faint surface texture details and swirl artifacts that are the result of aliasing due to a slight mismatch between the scan direction and the focal plane orientation.

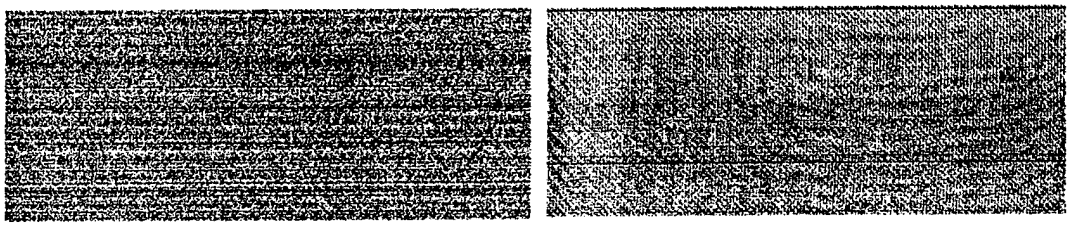

Rearranged; stdev = 8.71 Polynomial reconstruction; stdev = 2.63

Figure .26 Typical difference between post-heating images at consecutive frames. In the rearranged image (left), focal plane fixed pattern noise appears as horizontal lines which do not appear in the polynomial reconstruction. The lower standard deviation in the reconstructed image reflects the decreased noise content.

Time derivates of the reconstructed sequences were examined as a means of improving the contrast between subsurface features and the background. Although a similar derivative scheme has been shown to be extremely effective in pulsed thermography, neither the first or second time derivatives images improved on the rearranged or raw sequences. In fact, the derivative images actually reduced, and often removed, all target background contrast.

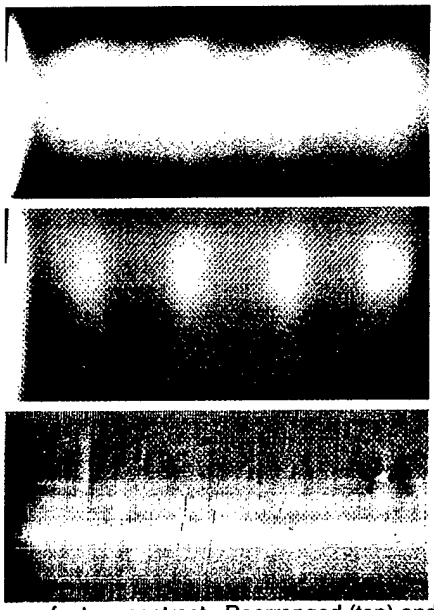

Figure 27. Effect of time derivatives on feature contrast. Rearranged (top) and background subtracted (center) images offer better contrast between the 4 subsurface holes and the background than the time derivative image, where all contrast is eliminated.

SIT Evaluation of a Carbon Fiber Test Panel

A flat bottom hole CFRP test panel was constructed and scanned to evaluate the performance of the SIT proof of concept system for detection of subsurface features. The panel was constructed from 32 ply CFRP prepreg, with holes machined in one side. The panel was designed to provide a set of subsurface features that range from easily detectable with a simple IR camera-heat gun setup, to those that are beyond the capability of current state of the art thermography technology. The key parameter for thermographic detectability of subsurface features is aspect ratio (diameter / depth). The widely used "rule of thumb" in thermography is that features with aspect ratios less than approximately 1-2 are generally undetectable, while features with aspect ratios greater than approximately 10 are easily detectable with a modest camera and heat source. It is in the intermediate range between these aspect ratios where thermographic NDT is most widely used. A motivation of this, and many other projects, is to allow thermography to be used for NDT of defects with aspect ratios smaller than 1-2. Features in the test panel spanned a range of aspect ratios from 0.6 to 12.2.

In typical experiments, the panel was scanned in 4 passes to allow sufficient spatial resolution for the entire range of defects. Each scan covered a row of holes with the same diameter. The scan was synchronized to camera acquisition so that the sample moved 0.020" with each acquired frame. Scan speeds were either 1 or 0.5 inches per second in various experiments (slower speeds were used in attempting to image deeper features). Data was acquired at a 50 Hz (or 25 Hz for 0.5 ips) frame rate. Typical induction frequencies were in the 200 kHz range with currents in the 0.5 – 3.0 A range.

Acquired data was archived in a raw format, and then rearranged and reconstructed using split 6^{th} order polynomials to fit the pre and post heating data using a least squares method. The entire process was done in a single pass using a program written in LabVIEW. The program allowed manipulation of various parameters and processing options, and saved the reconstructed results as a single continuous data structure (the blind interval due to the coil pass was eliminated). In general, we found that there was no benefit obtained by using polynomials with order greater than 6. Although numerous processing schemes were tested, none outperformed relatively simple background subtraction using the pre-heating frames for background. Refinements to background subtraction,

including iterative median filtering of the background image and weighted subtraction were implemented, although these only served to make detectable features more distinct from that background; they did not allow retrieval of previously undetectable features.

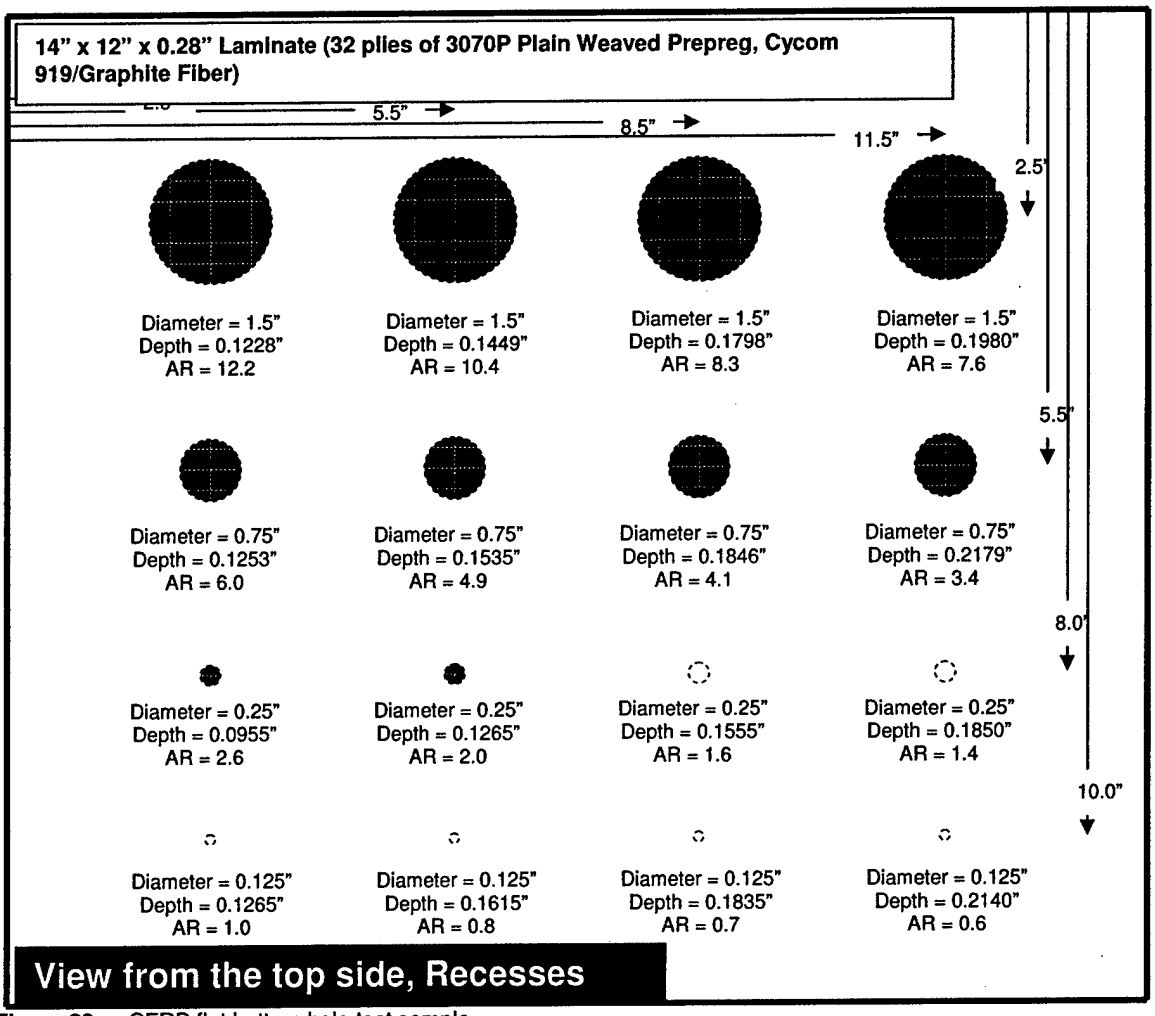

Figure 28. CFRP flat bottom hole test sample

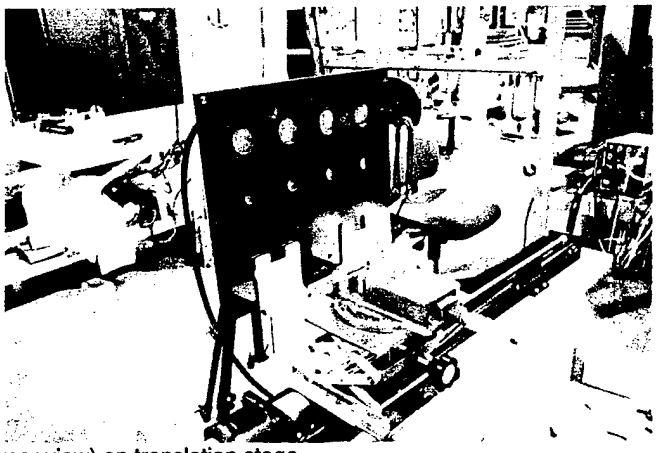

Figure 29. Test panel (rear view) on translation stage.

Data from a typical scan experiment is shown in Fig. 30, in which the test panel was imaged in four passes so that each row of same-diameter holes was acquired separately. Examination of the results led to the following observations:

1. Subsurface features with aspect ratio greater than approximately 2.6 were detectable.
2. Shape and size information about the subsurface features was not clearly indicated. Defects with 0.25 and 1.5" diameter presented similar temperature profiles at the sample surface.
3. An artificial hot spot was routinely created at the sample edge at the end of the scan line.
4. Heating of the sample by the paperclip-shaped coil was not uniform along the coil. There was typically a stripe along the center of the scan axis in which the temperature was highest.
5. Contrast between a subsurface feature and the background occurred after the passage of the coil over that feature. No substantial contrast occurred during the temperature rise as the coil approached that point.
6. Feature-background contrast developed during a 1-2 second interval after passage of the coil over the feature. After that time, the contrast persisted and changed very slowly in time.

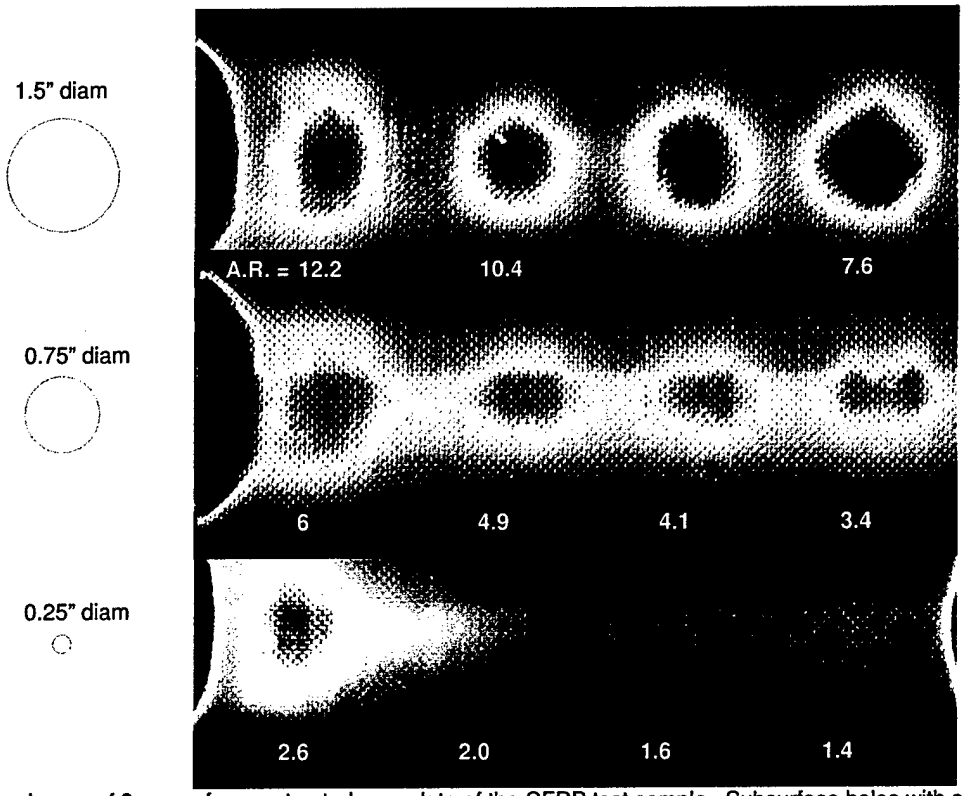

Figure 30. Image of 3 rows of reconstructed scan data of the CFRP test sample. Subsurface holes with aspect ratio > 2 were detected, although feature shapes were indistinct.

It is possible to improve the shape-size retrieval characteristics of the SIT images by considering the behavior of each pixel in the brief interval immediately after the passage of the coil (Fig. 31). In the 2 frames after the passage of the coil, pixels located on defect-free points show a brief drop in temperature, followed by a gradual rise. However, pixels located over subsurface defects do not experience this temperature drop, and rise to an asymptotic temperature value that decays slowly. The temperature differences between defect and non-defect pixels during this post-heating interval are small, so that images acquired in this interval do not improve defect resolution. However, images of the time derivative of each pixel during this interval show defect pixels with different polarity than defect free pixels

(defect pixels have positive slopes, defect-free slopes are negative) so the difference is readily apparent. For these images, the slope is calculated from the rearranged data (no polynomial fit), so no noise reduction is applied. The slope is a simple linear fit to the 2 frames immediately following the coil passage. Although this approach offers improved resolution of defect shape and size, it is less sensitive to low aspect ratio defects than the polynomial with background subtraction strategy.

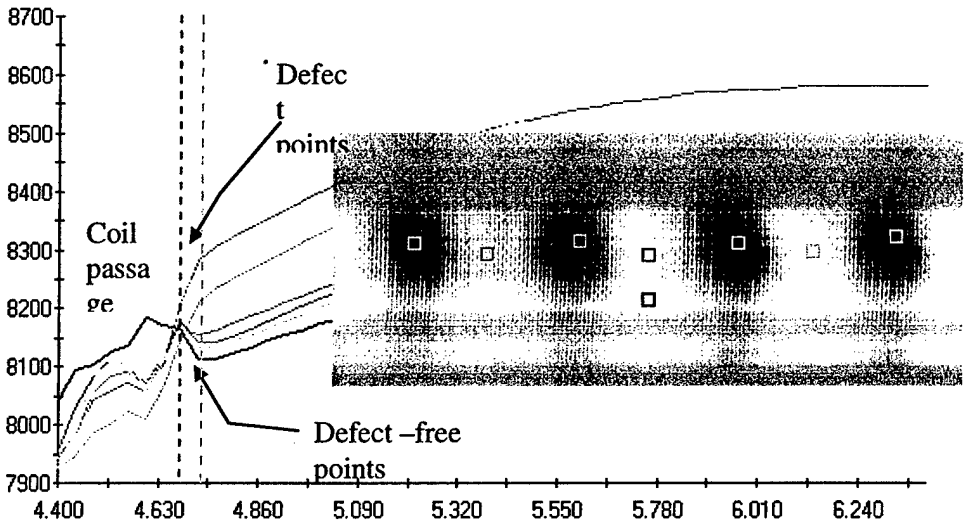

Figure 31. Temperature time curve shows that immediately after coil passage, defect points rise in temperature while defect-free points fall. The image shows the slope of each pixel during the 2-frame interval indicated in the plot.

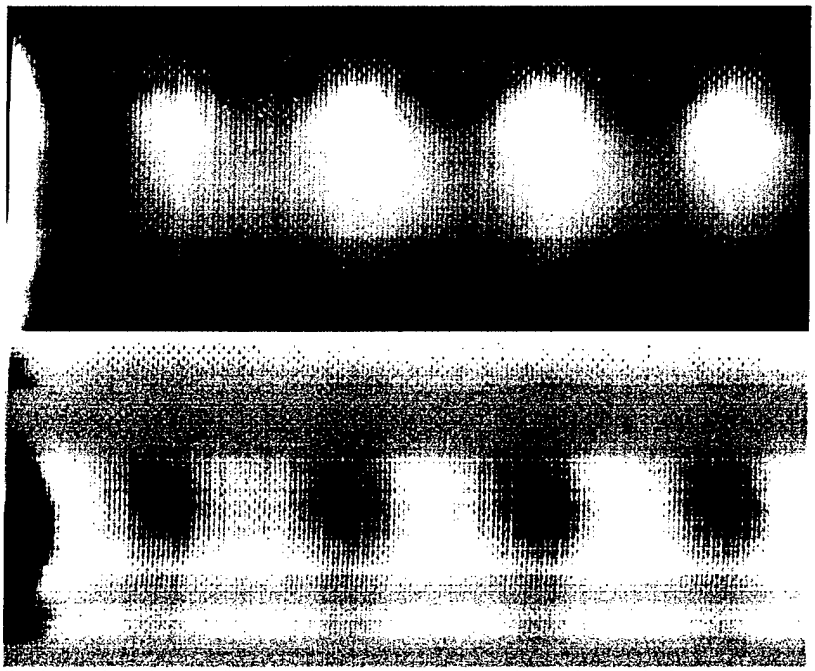

Figure 32. Amplitude (top) and slope (bottom) images during the 2 frame interval after coil passage for a row of 1.5" diameter holes. The circular subsurface features are indistinct in the amplitude image, but they appear clearly, with inverted polarity in the slope image.

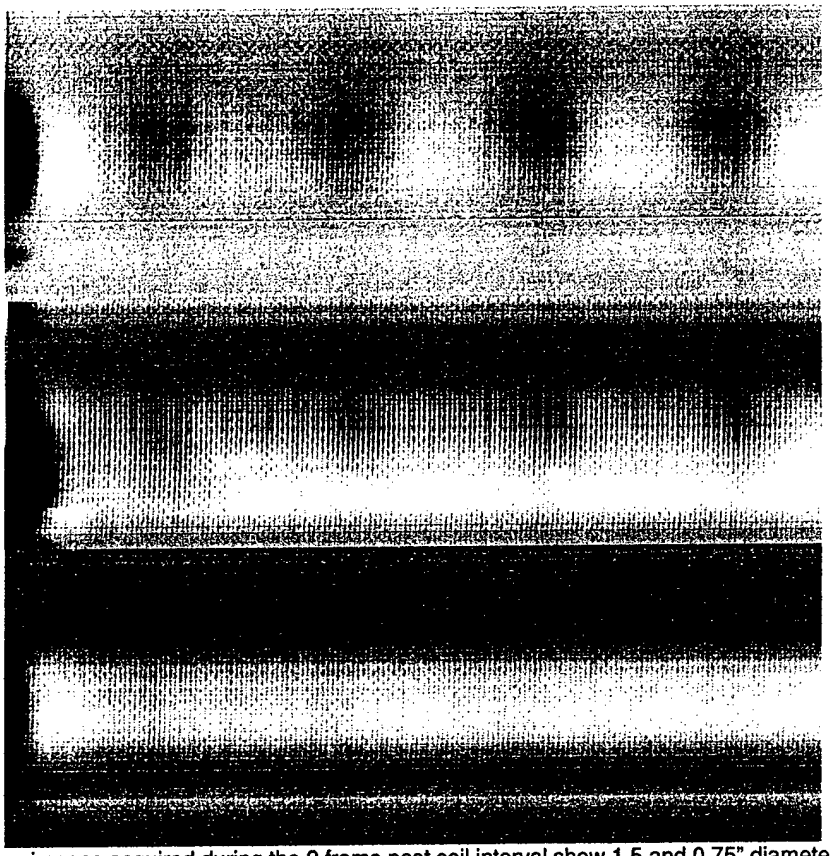

Figure 33. Slope images acquired during the 2 frame post coil interval show 1.5 and 0.75" diameter features, although no 0.25" features were detected.

Detection of low aspect ratio features can be improved by increasing the heating amplitude, which can be accomplished by increasing the induction current, reducing the scan speed, or placing the coil closer to the sample surface. The effect of the increased heating is not readily apparent in the raw or rearranged images, and in fact, these images may actually contain additional artifacts, as emitted radiation from the sample surface is reflected off of surfaces in the vicinity of the sample. However, the post-coil passage transient slope images remove most of the clutter. In fact, we were able to image features with aspect ratios as low as 1.4 using 3 amp coil current and the slope processing method.

The extent to which the heating amplitude can be increased is limited in practice by the dynamic range of the infrared camera. Although the differential temperatures on a sample between subsurface features and benign areas of the sample were small (< 5 C), the overall temperature of the sample was raised considerably. At 3 A coil current (the practical limit for our experiments), the response of the IR camera was saturated. We estimate that at the point of saturation, the sample surface temperature had reached 50 C.

The combined effects of increased coil current and post coil-pass slope processing made it possible to detect 0.25" diameter features in the flat bottom hole test sample. For the smaller features (e.g. aspect ratio = 1.6 and 1.4), the images of the subsurface features are indistinct. However, examination of the slope amplitudes along a line that bisects all 4 holes in the row confirms the correlation between decreased slope value and subsurface features (Fig. 34). Unfortunately, the slope images are sensitive to the small variations in emissivity that occur as a result of the sample surface texture. These appear in the images in Fig. 35 as fine vertical lines and an even finer cross-hatch pattern. (these should not be confused with scan artifacts, which appear as horizontal lines across the entire sample). The images can be improved by simple image processing, e.g. an iterative median filter. However, mean filtering should be avoided, as it tends to further obscure sample edges and shapes.

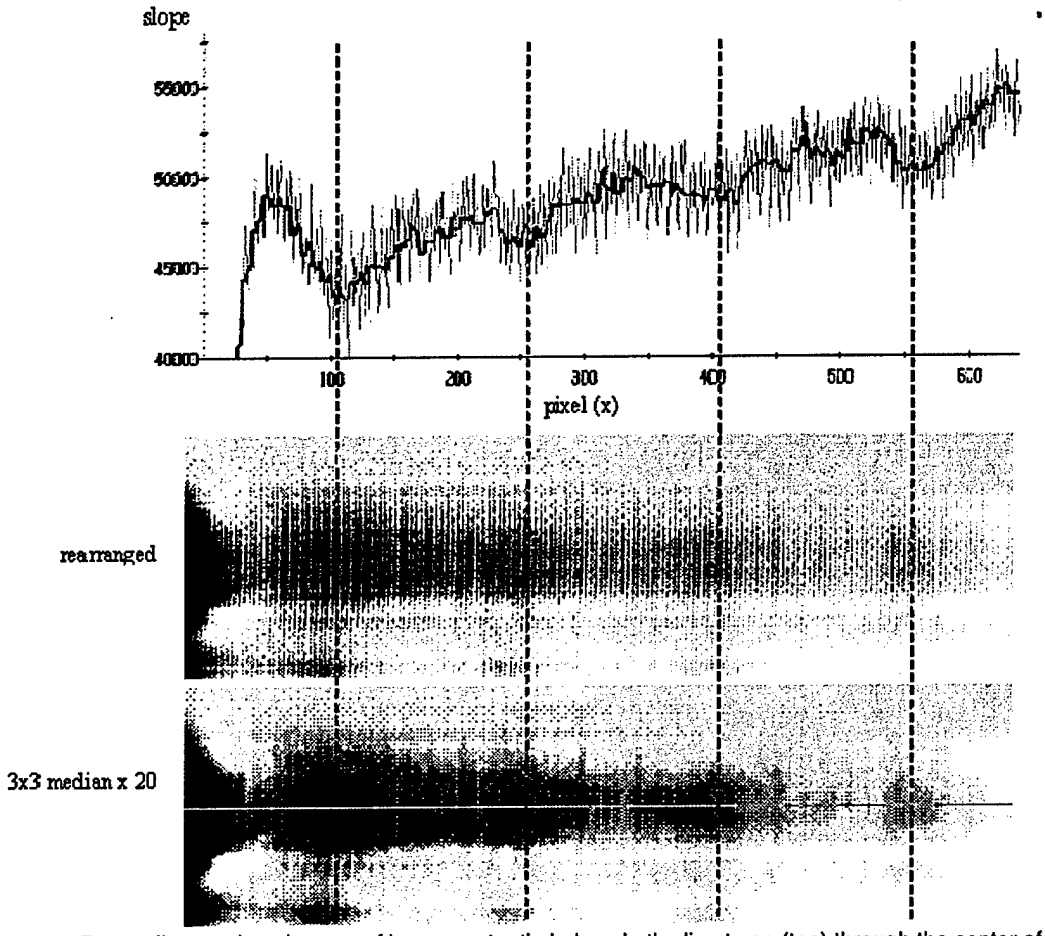

Figure 34. Post-coil pass slope images of low aspect ratio holes. In the line trace (top) through the center of the sample, the slope amplitude of the holes decreases. The line trace of the rearranged data (red trace, center image) is susceptible to noise, which is greatly reduced by a 3x3 median filter with 20 iterations (black trace, bottom image).

Comparison with Pulsed Thermography

In order to establish a performance baseline for the SIT system, samples were evaluated using a commercial flashlamp-based Pulsed Thermography system (EchoTherm). The PT system uses 2 linear flashtubes to deliver approximately 10 kJoules to the sample surface. Approximately 10 seconds of data was collected for the CFRP flat bottom holes sample, and the data was processed using the Thermographic Signal Reconstruction method built into the Mosaiq software, which is part of the PT system. We used this system because it is representative of how thermography is currently used for inspection of aerospace composites in both manufacturing and maintenance applications. The results of the PT inspection are shown in Fig. 35. The results are roughly comparable, for although the PT images are sharper and more distinct, we were ultimately able to image lower aspect ratio features with the SIT system. It is also important to note that neither system was capable of imaging features with aspect ratio less than 1.

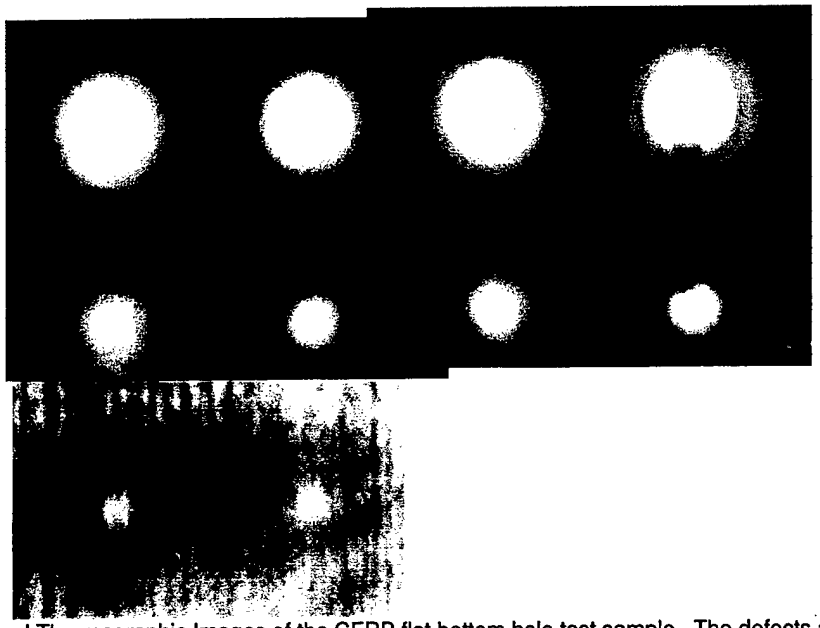

Figure 35. Pulsed Thermographic Images of the CFRP flat bottom hole test sample. The defects are more distinct, however SIT did image lower aspect ratio features.

Discussion

Our objective in Phase I was to evaluate the feasibility of Scanning Induction Thermography for the evaluation of carbon fiber based composites. We also had a particular interest in the ability to detect low aspect ratio features, as this is a capability that is not possible with currently available flash-based thermographic NDT systems. In the modeling efforts in Phase I, it was demonstrated that small irregularities in the bulk of a CFRP sample should generate a detectable perturbation to the resultant surface temperature distribution when an appropriate magnetic field gradient is applied. However, in subsequent experiments the SIT results were actually less sensitive to subsurface features than Pulsed Thermography, although signal-processing methods were developed and implemented to provide sensitivity similar to, and perhaps slightly better than Pulsed Thermography. Initially, this discrepancy between model results and experiment was surprising, as we had every expectation that the SIT system would significantly outperform the PT system for detection of low aspect ratio features in CFRP. However, further analysis of both modeling and experimental data fully explains the results of the program, and also suggests logical steps for further investigation.

Modeling in Phase I was performed to confirm the interaction between an applied field and a CFRP sample, and specifically, to determine the anticipated surface temperature response for various conditions such as holes and slots. The flaws were modeled to extend through the entire thickness of the sample. The resultant temperature distribution is calculated based on the heat generated by one of the three mechanisms identified (Joule heating, dielectric hysteresis or fiber contact). Regardless of which of the three mechanisms applies to a particular sample, the interaction between field and sample is presumed to be direct and instantaneous, i.e. the response of the material closely follows changes in the applied field. Thermal diffusion was not taken into account.

Our experimental results follow from this scenario, particularly when considering the difference between modeled results for a through-thickness hole and experimental results for a subsurface flat bottom hole. Modeling and subsequent experiments show a surface temperature gradient on either side of a through-thickness slot or hole under the magnetic field gradient. It is important to realize that the temperature gradient occurs in the immediate vicinity of the discontinuity in the material, so that a defect such as a round hole in an extended field can be considered to behave as an annular ring., or perhaps more accurately, a cylindrical shell. This is of little consequence if the feature extends through the sample thickness. However, if the defect is buried, from a heat transfer point of view it behaves as a line source, and not as a disk. This has serious implications in terms of detectability, as the surface temperature contrast of a buried feature will ultimately depend on its aspect ratio. A buried line source is inherently a low aspect

ratio structure compared to the disk it encloses. Although the aspect ratio of a disk depends on diameter and depth of the disk, this will not hold true for the ring or cylinder, where only the line or wall thickness is a factor.

The interaction we have described is quite different from conventional thermographic NDT processes, where a larger defect diameter always improves detectability. In the instance we are describing, it is likely that contrast will worsen as diameter increases, as there is progressively less superposition of heat from the line segments along the annulus as diameter increases. In fact, it is also likely that as diameter decreases, one might expect some improvement in contrast, since the annulus will converge and begin to resemble a small disk.

In the scanned experimental results, we see continuous regions of elevated temperature behavior, as opposed to the rings that we might expect from modeling predictions. This behavior also follows from the same considerations. The magnetic field causes heat to be generated instantaneously around the perimeter of the subsurface hole. The resultant heated ring immediately begins to diffuse in all available directions, including toward the center of the disk. Heat traveling away from the disk is free to diffuse throughout the bulk of the sample. However, heat traveling onto the disk is trapped between the disk and the surface, where it raises the surface temperature in the immediate area.

The interaction we have described offers an explanation for the apparent discrepancy between model results for through-hole features and experimental results with buried features. We see that even though the SIT heat generation mechanisms are near-instantaneous, and are able to penetrate CFRP and many other materials far more readily than a light pulse applied to the sample surface, the *contrast generation* mechanisms for both SIT and pulsed thermography are essentially the same; heat is trapped between the feature and sample surfaces, causing a local temperature surface temperature increase. Thus, the aspect ratio of the defect is a factor for SIT detectability, as it determines the size and persistence of the trap (trapped heat escapes quickly from a low aspect ratio defect, and much more slowly from a larger one).

Despite the constraints described above, the proof of concept system was able to achieve results that were toughly comparable to a pulsed thermography system, and in fact, the SIT system ultimately demonstrated better sensitivity to low aspect ratio features. Based on the experience gained in Phase I, we believe that it is possible to make additional improvements that would significantly enhance performance. Most importantly, we would base future efforts on exploitation of the interaction that occurs immediately after, and perhaps during, the passage of the heating coil over a given stripe on the sample. The rearranged sequences allowed us to exploit the inverted polarity during this period, and the system could be modified to allow more data to be acquired during this time when transient heat flow is at a maximum (just as heat generation by a magnetic field is at a maximum in a spatial field gradient, thermographic detection of subsurface features is best achieved when transient heat flow is at a maximum).

In a follow-up effort, we would also redirect the focus of the modeling effort towards understanding diffusion heat from closed loop line heat sources into an enclosed heat trap, and the dynamics of this process.